ORNL/TM--9075

DE84 013627

Fusion Energy Division

PROPAGATION AND ABSORPTION OF ELECTROMAGNETIC WAVES IN FULLY RELATIVISTIC PLASMAS

D. B. Batchelor

R. C. Goldfinger
Computer Sciences

H. Weitzner
New York University

Date Published - May 1984

Prepared by the
OAK RIDGE NATIONAL LABORATORY
Oak Ridge, Tennessee 37830
operated by
Martin Marietta Energy Systems, Inc.
for the
U.S. DEPARTMENT OF ENERGY
under Contract No. DE-AC05-840R21400

CONTENTS

ABSTRACT

The propagation and absorption of electromagnetic waves in a relativistic Maxwellian plasma are investigated by solving the uniform plasma dispersion relation. Both the Hermitian and the anti-Hermitian parts of the plasma conductivity tensor $\underset{\approx}{\sigma}$ are calculated relativistically. The Bessel functions occurring in $\underset{\approx}{\sigma}$ are not expanded, and many cyclotron harmonic terms are included at high temperatures. The dispersion relation is solved numerically for perpendicular propagation, $k_{\parallel} = 0$, where the relativistic effects are maximum and are not masked by Doppler broadening, which has been more thoroughly investigated. It is found that relativistic broadening has a substantial effect on wave dispersion, shifting the extraordinary mode right-hand cutoff and the upper hybrid resonance to a higher magnetic field with increasing temperature. Above a critical temperature the cutoff disappears entirely. There is a broad range of temperatures, 20 keV $\lesssim T_e \lesssim$ 500 keV, for which the wave number $k_{\perp}$ differs significantly from both the cold plasma value and the vacuum value. This has important implications for ray tracing in relativistic plasmas. Wave damping rates are calculated and compared to results from a previous formulation using the Poynting theorem, in which only the Hermitian part of $\underset{\approx}{\sigma}$ is calculated relativistically.

I. INTRODUCTION

In investigating electromagnetic wave propagation in very high temperature plasmas, $T_e \sim m_e c^2$, two important modifications to the usual warm plasma wave theory must be included. First, the relativistic variation of mass with energy $m = \gamma(E) m_e$ broadens the cyclotron resonances $\sim(\omega - k_\parallel v_\parallel/\gamma - \ell\Omega_e/\gamma)^{-1}$. Second, finite Larmor radius effects $k_\perp \rho_e$ associated with the large particle energies cause high-order cyclotron harmonics $\ell\Omega_e$ to make important contributions to the plasma response even at relatively low wave frequencies $\omega \sim \Omega_e$.

In most cases of interest in fusion research, electron temperatures are limited to $T_e \leq 20$ keV. In this weakly relativistic regime, $\gamma \simeq 1$, Doppler broadening dominates relativistic effects except for very nearly perpendicular propagation, $n_\parallel^2 \leq T_e/m_e c^2$ and $n_\parallel^2 \leq 1 - \Omega_e^2/\omega^2$. Also, $k_\perp \rho_e$ generally remains small so that higher, nonresonant cyclotron harmonics make a negligible contribution to the plasma response. Now there is quite an extensive literature on electromagnetic wave propagation in weakly relativistic plasmas. Trubnikov[1] derived an expression for the plasma conductivity tensor of a relativistic Maxwellian plasma. This expression involves infinite integrals over MacDonald functions that are quite difficult to evaluate numerically. Dnestrovskii et al.[2] and especially Shkarofsky[3] derived from Trubnikov's expression a weakly relativistic limit in which cyclotron harmonics are treated individually and velocity space integrals are represented in terms of the $F_\ell(z)$ and $F_\ell(z,n_\parallel)$ functions (see Ref. 3). Since that time a number of alternative formulations of the weakly relativistic problem have appeared,[4,5] and numerous authors have used these results to calculate damping rates and investigate heating in specific devices. For a comprehensive collection of references see Ref. 6.

However, there exists a class of devices in which microwaves are used to produce very energetic populations, $T_e \sim m_e c^2$ (Ref. 7). For example, in the ELMO Bumpy Torus-Scale (EBT-S) device electron temperatures of 500 keV are obtained routinely, and scaling arguments indicate that temperatures of order 1 MeV are to be expected in future EBT devices such as the EBT Proof of Principle (EBT-P). In addition, hot electrons are essential to the operation of thermal barriers in tandem mirrors. The electron cyclotron resonance heating (ECRH) must establish and maintain an average hot electron energy of $\simeq$450 keV in the thermal barrier and a temperature of $\simeq$70 keV in the end plug.[8] Hot electron temperatures of up to 650 keV are being discussed for the Mirror Advanced Reactor Study (MARS) tandem mirror reactor. At temperatures such as this the weakly relativistic expansion

$\gamma(p) = (1 + p^2/m^2c^2)^{1/2} \simeq 1 + p^2/2m^2c^2$ certainly breaks down. The cyclotron harmonics are broadened until individual harmonics overlap and are washed out. Also, high harmonics contribute to the plasma response, up to $l \geq 40$, depending on Ω_e/ω. Clearly, a fully relativistic treatment is required.

In order to study hot electron ring heating in EBT devices a fully relativistic wave damping model was developed for use in the RAYS geometrical optics code.[9] This model was based on the Poynting theorem,

$$\frac{d}{ds}\,|\underset{\sim}{S}| = \frac{4\pi}{c}\,\underset{\sim}{E}^{*} \cdot \underset{\approx}{\sigma}^{H} \cdot \underset{\sim}{E} \ . \tag{1.1}$$

Here, s is the arc length along a ray, $\underset{\sim}{S} = \mathrm{Re}[\underset{\sim}{E}^{*} \times (\underset{\sim}{n} \times \underset{\sim}{E})]$ = Poynting vector, $\underset{\sim}{n} = c\,\underset{\sim}{k}/\omega$ = real refractive index, $\underset{\sim}{E}$ = wave electric field amplitude, and $\underset{\approx}{\sigma}^{H}$ = Hermitian part of the relativistic conductivity tensor. The real refractive index is determined from the ray-tracing code, which uses the cold plasma dispersion relation

$$D(\underset{\sim}{n}) = \det(\underset{\approx}{D}) = \det\left[(1 - n^2)\,\underset{\approx}{I} + \underset{\sim\sim}{n\,n} + \frac{4\pi_I}{\omega}\,\underset{\approx}{\sigma}^{A}(\underset{\sim}{n})\right] = 0 \ , \tag{1.2}$$

where $\underset{\approx}{\sigma}^{A}$ = anti-Hermitian part of the plasma conductivity. Two plasma components are included in $\underset{\approx}{\sigma}^{A}$: a cold core plasma component and an annulus component, for which $\underset{\approx}{\sigma}^{A}$ is also assumed to be of the cold form. The electric field eigenvectors $\underset{\sim}{E}$ used in the equation are determined from the cold plasma dispersion tensor with both components included, $\underset{\approx}{D} \cdot \underset{\sim}{E} = 0$. In calculating $\underset{\approx}{\sigma}^{H}$ an isotropic relativistic Maxwellian distribution function is assumed:

$$\underset{\sim}{F}(p) = \frac{1}{m^3c^3}\,\frac{\rho n_e}{4\pi K_2(\rho)}\,\exp\left[-\rho\left(1 + \frac{p_\parallel^2 + p_\perp^2}{m^2c^2}\right)^{1/2}\right] \ , \tag{1.3}$$

where $\rho = m_e c^2/T_e$ and $K_2(\rho)$ is the modified Bessel function. An arbitrary number of cyclotron harmonics can be retained, and all Bessel functions containing finite Larmor radius effects are included without expansion.

The rings in EBT form at the second harmonic cyclotron resonance and are confined well away from the fundamental cyclotron resonance (see Fig. 1 of Ref. 9). Since the density of the hot electron plasma component is typically a small fraction of the cold ($T_e \leqslant 500$ eV) core component, it was felt that the real part of $\underset{\sim}{k}$ and the electric field polarization $\underset{\sim}{E}$ would be adequately described by the cold plasma dielectric tensor equation (1.2) near the second harmonic resonance. This procedure clearly breaks down near the fundamental resonance, because even nonrelativistically there are important finite temperature modifications to $\underset{\sim}{k}_r$ and $\underset{\approx}{E}$ when $\omega \sim \Omega_e$. Applications of this model to EBT devices have been presented in Ref. 9. A Poynting theorem approach similar to this was employed to calculate opacity to synchrotron radiation in Ref. 10.

In order to justify the validity of our Poynting theorem model for EBT and to investigate predominantly hot electron plasmas such as those in tandem mirror thermal barriers, a code was developed in which $\underset{\approx}{\sigma}^A$, as well as $\underset{\approx}{\sigma}^H$, is calculated relativistically. By solving the relativistic dispersion relation we can compute the correct values of $\underset{\sim}{k}_r$ and $\underset{\sim}{k}_i$, and by solving the dispersion tensor with the relativistic $\underset{\sim}{k}$ we obtain accurate polarization eigenvectors. With this code, we have addressed a number of questions arising from the relativistic effects: At what temperature do the relativistic modifications become important, and, for a given temperature, how many harmonics must be included in $\underset{\approx}{\sigma}^A$ and $\underset{\approx}{\sigma}^H$? What effect does high temperature have on qualitative features of wave propagation such as cutoffs, resonances, and polarization? From simple arguments one would expect that as the relativistic electron mass increases, the plasma refraction would decrease. This is borne out in calculations that show the real part of the wave refractive index n_r changing from the cold plasma value at low temperature to the vacuum value at sufficiently high temperature. These results indicate when cold plasma ray-tracing results are likely to be valid.

In this paper we investigate waves in a relativistic Maxwellian plasma described by Eq. (1.3). We have restricted consideration to perpendicular propagation, $n_\parallel = 0$, in order to emphasize the effect of relativity over the better understood

effects of Doppler shift and because of the large amount of computer time required to evaluate and solve the dispersion relation. In Sec. II, we derive the relativistic conductivity tensor in a form suitable for computation and specialize to $n_{\|} = 0$. In Sec. III, we give solutions of the dispersion relation for various magnetic fields and plasma densities, indicating the behavior of the propagation constant k_r and absorption rate k_i for increasing temperature. In Sec. IV, we compare damping rate calculations obtained using the full dispersion relation with those using the Poynting theorem. The results are summarized and conclusions discussed in Sec. V.

II. DERIVATION OF THE RELATIVISTIC CONDUCTIVITY TENSOR

Electromagnetic waves in a relativistic plasma are described by the Vlasov-Maxwell system:

$$\nabla \times \underset{\sim}{E} = -\frac{1}{c}\frac{\partial \underset{\sim}{B}}{\partial t} ,$$

$$\nabla \times \underset{\sim}{B} = \frac{1}{c}\frac{\partial \underset{\sim}{E}}{\partial t} + \frac{4\pi}{c}\underset{\sim}{J} ,$$

$$\frac{\partial f_j}{\partial t} + \nabla \cdot (\underset{\sim}{v} f_j) + \nabla_p \cdot (\dot{\underset{\sim}{p}}_j f_j) = 0 , \tag{2.1}$$

$$\underset{\sim}{J} = \sum_j e_j \int d^3p \, \underset{\sim}{v} f_j(\underset{\sim}{p}) ,$$

$$\dot{\underset{\sim}{p}}_j = \frac{e_j}{m_j}\left(\underset{\sim}{E} + \frac{\underset{\sim}{v}}{c} \times \underset{\sim}{B}\right) ,$$

where $\underset{\sim}{p} = \gamma m \underset{\sim}{v}$, $\gamma = (1 - v^2/c^2)^{-1/2} = (1 + p^2/m^2c^2)^{1/2}$, e_j = charge of jth particle species, and m_j = mass of jth species. In this paper, only electrons are considered so that $e_j = e = -|e|$ and $m_j = m_e = m$. We investigate plane waves propagating in a uniform plasma with equilibrium magnetic field B in the z direction, $\underset{\sim}{B}^0 = B^0\hat{z}$, and equilibrium distribution function $F(\underset{\sim}{v})$. The perturbed quantities are then of the form

$$\underset{\sim}{E}(\underset{\sim}{x},t) = \hat{\underset{\sim}{E}} e^{i(\underset{\sim}{k}\cdot\underset{\sim}{x} - \omega t)} ,$$

$$\underset{\sim}{B}(\underset{\sim}{x},t) = \frac{c}{\omega}\underset{\sim}{k} \times \underset{\sim}{E}(\underset{\sim}{x},t) , \tag{2.2}$$

$$f(\underset{\sim}{x},\underset{\sim}{v},t) = \hat{f}(\underset{\sim}{v}) e^{i(\underset{\sim}{k}\cdot\underset{\sim}{x} - \omega t)} .$$

With this ansatz the linearized Vlasov equation becomes

$$-i\left(\omega - \frac{1}{\gamma m}\,\underset{\sim}{p}\cdot\underset{\sim}{k}\right)\hat{f} - \frac{\Omega_0}{\gamma}(\underset{\sim}{p}\times\hat{z})\cdot\frac{\partial\hat{f}}{\partial\underset{\sim}{p}}$$

$$- e\left(\underset{\sim}{E} + \frac{1}{\gamma mc}\,\underset{\sim}{p}\times\underset{\sim}{B}\right)\cdot\frac{\partial F}{\partial\underset{\sim}{p}} = 0\ , \tag{2.3}$$

where $\Omega_0 = eB^0/mc < 0$ is the nonrelativistic cyclotron frequency. The manipulations necessary to solve Eq. (2.3) for $\hat{f}$ are quite standard and can be found in many textbooks. The plasma current can be expressed as

$$\underset{\sim}{J} = e\int d^3p\ \underset{\sim}{v}\hat{f}(\underset{\sim}{p})e^{i(k\cdot x-\omega t)} = \underset{\approx}{\sigma}\cdot\underset{\sim}{E}\ , \tag{2.4}$$

which is then used in Maxwell's equations to give the dispersion equation

$$\underset{\approx}{D}\cdot\underset{\sim}{\hat{E}} = \left[(1-n^2)\,\underset{\approx}{I} + \underset{\sim}{n}\,\underset{\sim}{n} + \frac{4\pi i}{\omega}\,\underset{\approx}{\sigma}\right]\cdot\underset{\sim}{\hat{E}} = 0 \tag{2.5}$$

and the dispersion relation

$$D(\underset{\sim}{n}) = \det[\underset{\approx}{D}] = 0\ .$$

For an isotropic equilibrium distribution, $F = F(\gamma)$, the form of the conductivity tensor is much simplified,

$$\underset{\approx}{\sigma} = \frac{2\pi e^2}{j\omega m}\int_0^\infty dp_z\int_0^\infty dp_\perp\,\frac{p_\perp}{\gamma(p)}\,(m^3c^3)\,\frac{\partial F}{\partial\gamma}\sum_l\frac{\underset{\approx}{M_l}(p)\ \underset{\sim}{\ }}{\gamma(p) - \dfrac{n_z p_z}{mc} - l\dfrac{\Omega_0}{\omega}}\ , \tag{2.6}$$

where

$$\underset{\sim}{M}_l(p_\perp,p_z) = \begin{bmatrix} \left(\frac{l\Omega_0}{n_\perp\omega}\right)^2 J_l^2 & i\frac{p_\perp}{mc}\left(\frac{l}{n_\perp}\frac{\Omega_0}{\omega}\right) J_l J_l' & \frac{p_z}{mc}\left(\frac{l}{n_\perp}\frac{\Omega_0}{\omega}\right) J_l^2 \\ -M_{xy} & \left(\frac{p_\perp}{mc}\right)^2 J_l'^2 & -i\frac{p_\perp p_z}{m^2c^2} J_l J_l' \\ M_{xy} & -M_{yz} & \left(\frac{p_z}{mc}\right)^2 J_l^2 \end{bmatrix},$$

where the J_l are Bessel functions of order l with argument $n_\perp(p_\perp/mc)(\omega/\Omega_0)$ and the p_z integration is taken over the usual Landau contour. For notational convenience we measure momentum in units of mc (that is, $p = mcp'$); we introduce a cyclotron frequency normalized to the wave frequency $\bar{\Omega} = |\Omega_0/\omega|$; and we renumber the index l such that positive harmonics are resonant for electrons, $l = -l'$. With these changes, when we drop the primes on p and l, Eq. (2.6) becomes

$$\underset{\approx}{\sigma} = \frac{2\pi e^2}{j\omega m}\int_0^\infty dp_\perp\, p_\perp \int_{-\infty}^\infty dp_z\, m^3c^3\, \frac{1}{\gamma}\frac{\partial F}{\partial \gamma} \sum_{l=-\infty}^{\infty} \frac{\underset{\approx}{M}_l}{\gamma - n_z p_z - l\bar{\Omega}},$$

(2.7)

where now

$$\underset{\approx}{M}_l = \begin{bmatrix} \left(\frac{l\bar{\Omega}}{n_\perp}\right)^2 J_l^2 & -i\frac{l\bar{\Omega}}{n_\perp} p_\perp J_l J_l' & \frac{l\bar{\Omega}}{n_\perp} p_z J_l^2 \\ -M_{xy} & p_\perp^2 J_l'^2 & ip_z p_\perp J_l J_\perp' \\ M_{xz} & -M_{yz} & p_z^2 J_l^2 \end{bmatrix}. \qquad (2.8)$$

The argument of the Bessel functions is $b = n_\perp p_\perp/\bar{\Omega} \geq 0$. To get Eq. (2.8) we have used $\Omega_0 = -|\Omega_0|$ and properties of Bessel functions $J_{-l}(z) = (-1)^l J_l(z)$, $J'_{-l}(z) = (-1)^l(z)$, $J_l(-z) = (-1)^l J_l(z)$, and $J_l'(-z) = (-1)^{l-1} J_l'(z)$.

To treat the singular resonance denominator in Eq. (2.7) we assume that ω is real and that n_z has a small positive imaginary part. Then the Plemelj relation gives

$$\frac{1}{\gamma - n_z p_z - l\bar{\Omega}} \rightarrow \mathbf{P}\left\{\frac{1}{\gamma - n_z p_z - l\bar{\Omega}}\right\} - i\pi\delta(\gamma - n_z p_z - l\bar{\Omega})$$

so that

$$\underset{\approx}{\sigma}^H = -\frac{2\pi^2 e^2}{\omega m}\int_0^\infty dp_\perp\, p_\perp \int_{-\infty}^\infty dp_z\, m^3c^3\,\frac{1}{\gamma}\,\frac{\partial F}{\partial \gamma}\,\underset{\approx}{M_l}\,\delta(\gamma - n_z p_z - l\bar{\Omega})\ , \tag{2.9}$$

$$\underset{\approx}{\sigma}^A = -i\,\frac{2\pi e^2}{\omega m}\,\mathbf{P}\int_0^\infty dp_\perp\, p_\perp \int_{-\infty}^\infty dp_z\, m^3c^3\,\frac{1}{\gamma}\,\frac{\partial F}{\partial \gamma}\,\frac{\underset{\approx}{M_l}}{\gamma - n_z p_z - l\bar{\Omega}}\ , \tag{2.10}$$

where **P** indicates a Cauchy principal value. It has proved convenient in the numerical computations to transform the integrals over p_z, $p_\perp$ to integrals over $p = (p_\perp^2 + p_z^2)^{1/2}$ and $\mu = \cos\chi$, where χ is the polar angle in velocity space, that is, $p_z = p\mu$ and $p_\perp = p(1 - \mu^2)^{1/2}$. When $n_\perp$ is real, $\underset{\approx}{\sigma}^H$ and $\underset{\approx}{\sigma}^A$ are, respectively, Hermitian and anti-Hermitian matrices.

Finally, we explicitly introduce the relativistic Maxwellian distribution function

$$F(\gamma) = \frac{n_e}{m^3c^3}\,\frac{\rho}{4\pi K_2(\rho)}\,e^{-\rho\gamma}\ , \tag{2.11}$$

where n_e = hot electron density, $K_2(\rho)$ = modified Bessel function, and $\rho = mc^2/T$ is an inverse temperature variable. At small energy (large ρ), Eq. (2.11) reduces to a nonrelativistic Maxwellian with temperature given by $T = mc^2/\rho$. At higher energy, expressing ρ in terms of the kinetic temperature is somewhat more complicated. With the distribution in Eq. (2.11) the average particle kinetic energy $\langle\epsilon\rangle$ can be expressed as

$$\langle \epsilon \rangle = \frac{1}{n_e} \int d^3p \; mc^2(\gamma - 1) F(\gamma) = mc^2 \left[\frac{3}{\rho} + \frac{K_1(\rho)}{K_2(\rho)} \right] . \qquad (2$$

Using the asymptotic expansions of $K_{1,2}$ for large ρ,

$$K_n(\rho) \sim \sqrt{\frac{\pi}{2\rho}} e^{-\rho} \left(1 + \frac{4n^2 - 1}{8\rho} + \ldots \right)$$

gives the usual nonrelativistic result,

$$\langle \epsilon \rangle = mc^2 \langle \gamma - 1 \rangle \sim \frac{3}{2} T \qquad \text{for } T/mc^2 \ll 1 , \qquad (2$$

while in the ultrarelativistic limit, $\rho = mc^2/T \ll 1$, the power series expan $K_n \sim 1/2\Gamma(n)(3/2)^n$, gives

$$\langle \epsilon \rangle = 5T - 1 \sim \frac{3}{2} \left(\frac{10}{3} T \right) \qquad \text{for } T/mc^2 \gg 1 . \qquad (2$$

In the intermediate range $\rho \simeq 1$, we find $\langle \epsilon \rangle \simeq 2.3T = 3/2(1.67)$ so that t thirds of the average particle energy when $T \simeq 500$ keV is about 800 keV.

The final form for the conductivity tensor used in all computations in this p is then

$$\underset{\approx}{\sigma}^H = \frac{\rho^2}{8K_2(\rho)} \frac{\omega_{pe}^2}{\omega} \sum_l \int_0^\infty dp \, \frac{p^2}{\gamma} \int_{-1}^1 d\mu \, \underset{\approx}{M_l}(p,\mu) \delta(\gamma - n_z p\mu - l\overline{\Omega}) , \qquad (2$$

$$\underset{\approx}{\sigma}^A = \frac{i}{\pi} \frac{\rho^2}{8K_2(\rho)} \frac{\omega_{pe}^2}{\omega} \sum_l \mathrm{P} \int_0^\infty dp \, \frac{p^2}{\gamma} e^{-p\gamma} \int_{-1}^1 d\mu \, \frac{\underset{\approx}{M_l}(p,\mu)}{\gamma - n_z p\mu - l\overline{\Omega}} .$$

(2

A. Computation of $\underset{\approx}{\sigma}^H$

The presence of the δ function permits one of the integrals in in Eq. (2.15) to be done immediately. It has proved convenient to do the p integral analytically and the μ integral numerically. Contributions to the p integral come from roots of the argument of the δ function, $f(p)$, where

$$f(p) = (1 + p^2)^{1/2} - n_z \mu p - i\bar{\Omega} \ . \tag{2.17}$$

Roots of this function can be visualized as the points of intersection of the hyperbola $y = (1 + p^2)^{1/2}$ with the line $y = i\bar{\Omega} + (n_z\mu)p$; see Fig. 1. Solving $f(p) = 0$ gives two roots:

$$p_\pm = \frac{i\bar{\Omega} n_z \mu \pm (i^2\bar{\Omega}^2 + n_z^2\mu^2 - 1)^{1/2}}{1 - n_z^2\mu^2} \ . \tag{2.18}$$

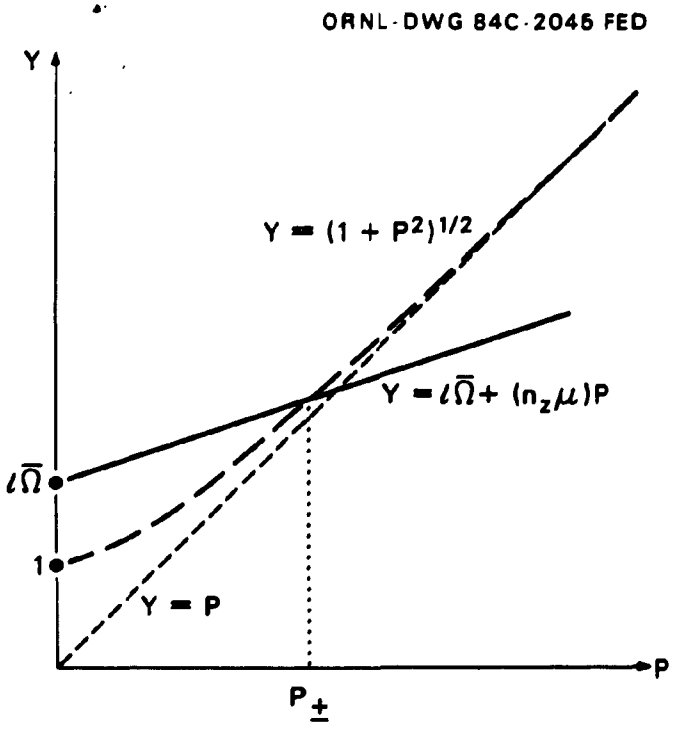

Fig. 1. Location of resonant values of momentum.

However, one or both solutions of Eq. (2.18) may be superfluous. A glance at Fig. 1 shows that we require three additional conditions:

1. p must be real, so the discriminant $\Delta = l^2\overline{\Omega}^2 + n_z^2\mu^2 - 1 \geq 0$,
2. p must be positive, so the root is within the right side of the hyperbola,
3. the root is on the top branch of the hyperbola, so $l\overline{\Omega} + n_z\mu p > 0$.

It is tedious to sort out these conditions algebraically, but the results can be easily understood with the help of Fig. 1. We group the results for varying $n_z\mu$ in four cases according to the relative cyclotron harmonic number $l\overline{\Omega}$ [i.e., the y intercept of the line $l\overline{\Omega} + (n_z\mu)p$].

Case 1.

$$\text{If } l\overline{\Omega} \leq 0 \ , \quad \begin{cases} \text{there are no valid roots for } n_z\mu \leq 1 \ , \\ p_- \text{ is a valid root for } n_z\mu > 1 \ . \end{cases}$$

Since $|\mu| \leq 1$ this implies that there are no resonant particles for zero or negative harmonics unless $n_z > 1$. That is, anomalous dispersion, $l < 0$, and inverse Cherenkov radiation, $l = 0$, are possible only if the parallel wave phase velocity is less than c.

Case 2.

$$\text{If } 0 < l\overline{\Omega} < 1 \ , \begin{cases} \text{there are no valid roots for } n_z\mu \leq (n_z\mu)_{\min} = (1 - l^2\overline{\Omega}^2)^{1/2} \ , \\ \text{there are 2 roots for } (n_z\mu)_{\min} \leq n_z\mu \leq 1 \ , \\ p_- \text{ is a valid root for } n_z\mu > 1 \ . \end{cases}$$

The value $(n_z\mu)_{\min}$ defines the point of tangency between the hyperbola and the line; that is, $\Delta = 0$ and $p_+ = p_-$.

Case 3.

$$\text{If } l\overline{\Omega} = 1 \ , \quad \begin{cases} p_+ = 0 \text{ is a valid root for } n_z\mu < 0 \ , \\ p_- = 0 \text{ and } p_+ > 0 \text{ are valid roots for } 0 \leqslant n_z\mu < 1 \ . \end{cases}$$

This is the case of exact cyclotron harmonic resonance. We see that there is always a root at $p = 0$; however, this root makes no contribution to the integral since the argument of the Bessel functions vanishes.

Case 4.

$$\text{If } l\overline{\Omega} > 1 \ , \quad \begin{cases} p_+ \text{ is a valid root for } n_z\mu < 1 \ , \\ \text{there are no valid roots for } n_z\mu \geqslant 1 \ . \end{cases}$$

Inspection of Fig. 1 also reveals the characteristic asymmetry with respect to Ω of the relativistic cyclotron absorption profile. Consider $n_z = 0$, in which case the moving line is horizontal, $y = l\overline{\Omega}$ for all μ. Then there are no intersections (resonant particles) below the harmonic ($l\overline{\Omega} < 1$), but there is an intersection at increasing p as $l\overline{\Omega}$ increases above 1. The increase of p_+ with $l\overline{\Omega}$ causes the strength of the resonance to be weighted by $J_l^2(n_\perp \overline{\Omega}\sqrt{1-\mu^2}p_+)$ for small p_+ and by the distribution function $\exp[-p(1 + p_+^2)^{1/2}]$ at large p_+. This produces the absorption line profile peaked above the cyclotron harmonic. For nonzero n_z the moving line slopes as μ ranges from $-1 \leqslant \mu \leqslant 1$, allowing some resonance below the cyclotron harmonic ($l\overline{\Omega} < 1$, $\mu > 0$) and permitting resonance with lower energy particles above the cyclotron harmonic ($l\overline{\Omega} > 1$, $\mu < 0$). The Doppler shift associated with n_z therefore tends to wash out the asymmetry of the relativistic shape. In the nonrelativistic limit one considers only the extreme left edge of Fig. 1 such that the hyperbola appears as the horizontal line $y = 1$. Then the absorption line shape is symmetric and determined entirely by the slope of the line $y = l\overline{\Omega} + (n_z\mu)p$, that is, Doppler shift.

Returning now to the evaluation of $\underset{\approx}{\sigma}^H$ we perform the p integration in Eq. (2.15) including the contribution of the roots of $f(p)$, Eq. (2.17), and obtain

$$\underset{\approx}{\sigma}^H = \frac{\rho^2}{8K_2(\rho)} \frac{\omega_{pe}^2}{\omega} \sum_{l=-\infty}^{\infty} \int d\mu \sum_{\pm} \frac{p_\pm^2}{\gamma(p_\pm)} e^{-\rho\gamma(p_\pm)} \frac{\underset{\approx}{M}_l(p_\pm,\mu)}{|f'(p_\pm)|} . \tag{2.19}$$

Using Eq. (2.17) we obtain $f'(p) = (p - \gamma n_z\mu)/\gamma$. Since $f(p) = 0$ implies $\gamma = n_z\mu p + l\overline{\Omega}$, this can be written $f'(p) = [(1 - n_z^2\mu^2)p_\pm - l\overline{\Omega}n_z\mu]/\gamma(p_\pm)$. Using Eq. (2.18) gives

$$f'(p_\pm) = \frac{\pm}{\gamma(p_\pm)} (l^2\overline{\Omega}^2 + n_z^2\mu^2 - 1)^{1/2} = \frac{\pm\Delta(\mu)}{\gamma(p_\pm)} . \tag{2.20}$$

The expression for $\underset{\approx}{\sigma}^H$ in Eq. (2.19) simplifies to

$$\underset{\approx}{\sigma}^H = \frac{\rho^2}{8K_2(\rho)} \frac{\omega_{pe}^2}{\omega} \sum_{l=-\infty}^{\infty} \int d\mu \sum_{\pm} e^{-\rho\gamma(p_\pm)} \frac{p_\pm^2 \underset{\approx}{M}_l(p_\pm,\mu)}{(l^2\overline{\Omega}^2 + n_z^2\mu^2 - 1)^{1/2}} , \tag{2.21}$$

where the range of integration over μ and the sum over $\pm$ are restricted by the existence of valid roots $p_\pm$ as discussed in the four cases above.

Case 1: $\overline{\Omega} < 0$. There is no contribution unless $n_z > 1$, in which case p_- is included and the range of integration is $1/n_z \leq \mu \leq 1$.

Case 2: $0 < \overline{\Omega} < 1$. Both $p_\pm$ are included and the range of integration is $\mu_{min} \leq \mu \leq 1$. It will be seen that the integrand in Eq. (2.21) has a singularity at $\mu = \mu_{min}$ associated with the degeneracy of $p_\pm$. The singularity is integrable, however, by making the change of variable

$$\mu = \frac{(1 - l^2\overline{\Omega}^2)^{1/2}}{|n_z|} \cos\theta , \quad \cos\theta = \frac{n_z\mu^2}{1 - l^2\overline{\Omega}^2} . \tag{2.22}$$

Then for values of l such that $0 < \mu_{min} = (1 - l^2\overline{\Omega^2})^{1/2}/n_z < 1$, the contribution to $\underset{\approx}{\sigma}^H$ is

$$\frac{\rho^2}{8K_2(\rho)} \frac{\omega_{pe}^2}{\omega} \sum_l \frac{1}{|n_\parallel|} \int_0^{\theta_{max}} d\theta \sum_\pm p_\pm^2 \underset{\approx}{M}_N[p_\pm, \mu(\theta)] \ , \tag{2.23}$$

where

$$\theta_{max} = \cos^{-1}\left[\left(\frac{n_z^2}{1 - l^2\overline{\Omega^2}}\right)^{1/2}\right] .$$

If $n_z > 1$, there is an additional contribution from p_- over the range $1/n_z \leq \mu \leq 1$.

Case 3: $l\overline{\Omega} = 1$. Exactly at cyclotron resonance the denominator in Eq. (2.21) vanishes at $\mu = 0$ (i.e., $\mu_{min} = 0$) and the transformation equation, Eq. (2.22), fails. However, the integrand is not actually singular since $p_\pm(\mu = 0)$ vanishes when $l\overline{\Omega} = 1$. In particular, we have $p_\pm = (n_z\mu \pm |n_z\mu|)/(1 - n_z^2\mu^2)$. Since $p_- < 0$, only p_+ contributes for $\mu \geq 0$ and we obtain for this particular l value

$$\frac{\rho^2 e^{-\rho}}{8K_2(\rho)} \frac{\omega_{pe}^2}{\omega} \int_0^1 d\mu \frac{4n_z\mu}{(1 - n_z^2\mu)^2} \underset{\approx}{M}_l(p_+, \mu) e^{-\gamma(p_+)} \ . \tag{2.24}$$

Case 4: $l\overline{\Omega} > 1$. Only p_+ contributes and the range of integration is $-1 \leq \mu \leq 1$.

A computer code has been written to evaluate $\underset{\approx}{\sigma}^H$ using Eqs. (2.21), (2.23), and (2.24). This code has been used with the Poynting theorem, Eq. (1.1), to investigate wave absorption by the hot electron rings in EBT devices. Results of these studies have been reported in Ref. 9.

In the following sections the full dispersion relation is solved for the special case $n_z = 0$. When $n_z = 0$, we have $p_+ = (l^2\overline{\Omega}^2 - 1)^{1/2}$, independent of μ, and the expression for $\underset{\approx}{\sigma}^H$, Eq. (2.21), is greatly simplified:

$$\underset{\approx}{\sigma}^H = \frac{\rho^2}{8K_2(\rho)} \frac{\omega_{pe}^2}{\omega} \sum_{l=l_{min}}^{\infty} (l^2\overline{\Omega}^2 - 1)^{1/2} e^{-\rho l\overline{\Omega}} \underset{\approx}{I}_l(p_+) \ , \tag{2.25}$$

where

$$\underset{\approx}{I}_l(p) = \int_{-1}^{1} d\mu \, \underset{\approx}{M}_l(p,\mu) \ . \tag{2.26}$$

Figure 2 shows the relative contribution of the various cyclotron harmonics to a typical element of $\underset{\approx}{\sigma}^H$, σ_{xx}^H, as a function of $\overline{\Omega} = |\Omega_0/\omega|$ for $T \simeq 40$ keV, $n_z = 0.0$, and $n_\perp = 1.0$. One can see considerable overlap in the higher harmonics, $l \gtrsim 2$, even though $n_z = 0$ and only relativistic line broadening is present. The absorption rate k_l tends to be proportional to the sum over l of $\sigma_{xx}^H(l)$, so the temperature dependence of the total σ^H is indicated by the plots of k_l [Fig. 4(b) below and Fig. 4 of Ref. 9].

B. Computation of $\underset{\approx}{\sigma}^A$

Computation of $\underset{\approx}{\sigma}^A$ is much more cumbersome and much more costly in computer time than $\underset{\approx}{\sigma}^H$ since two velocity space integrals must be performed numerically. It has proved convenient to perform the μ integral in Eq. (2.16) first,

$$\underset{\approx}{\sigma}^A = \frac{i}{\pi} \frac{\rho^2}{8K_2(\rho)} \frac{\omega_{pe}^2}{\omega} \sum_l \int_0^\infty dp \, \frac{p^2}{\gamma} e^{-\rho\gamma(p)} \underset{\approx}{I}_l(p) \ , \tag{2.27}$$

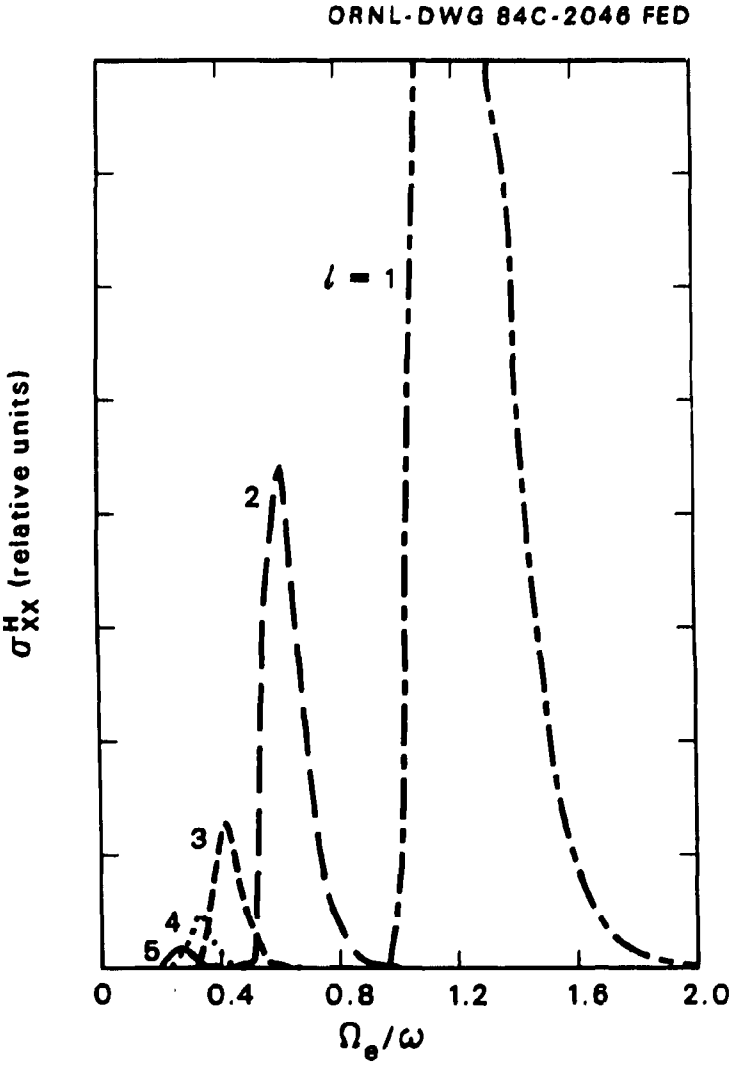

Fig. 2. Contributions of various cyclotron harmonics to σ^H_{xx}. Here $T_e = 40$ keV, $n_z = 0$, $n_\perp = 1.0$.

where

$$\underset{\approx}{I}_l(p) = -\frac{1}{n_z p} \mathbf{P} \, d\mu \int_{-1}^{1} \int_{-1}^{1} \frac{\underset{\approx}{M}_l(p,\mu)}{\mu - \mu_0} \, , \tag{2.28}$$

$$\mu_0 = \frac{1}{n_z p} [\gamma(p) - l\overline{\Omega}] \, . \tag{2.29}$$

There are three cases depending on the value of μ_0.

Case 1: $|\mu_0| > 1$. The μ integral is regular.

Case 2: $|\mu_0| = 1$. The μ integrand has a singularity at the upper or lower limit. This singularity is not integrable for $l = 0$ although the integral over p does still converge.

Case 3: $|\mu_0| < 1$. The μ integral is Cauchy.

Again, there is considerable simplification if $n_z = 0$. Then the resonant denominator is independent of μ, and $\underset{\approx}{\sigma}^A$ is

$$\underset{\approx}{\sigma}^A = \frac{i}{\pi}\frac{\rho^2}{8K_2(\rho)}\frac{\omega_{pe}^2}{\omega}\sum_l \mathrm{P}\int_0^\infty dp\,\frac{p^2 e^{-\rho\gamma}}{\gamma(\gamma - l\bar{\Omega})}\underset{\approx}{I}_l(p)\ , \tag{2.30}$$

where $\underset{\approx}{I}_l(p)$ was defined in Eq. (2.26). Again, one must consider three separate cases depending on $l\bar{\Omega}$ (refer again to Fig. 1).

Case 1: $l\bar{\Omega} < 1$. The p integrand is regular, and there are no resonant particles.

Case 2: $l\bar{\Omega} = 1$. The p integrand has an integrable singularity at $p = 0$.

Case 3: $l\bar{\Omega} > 1$. The integral is Cauchy.

In case 2, we make a change of variable to $x = \sqrt{\gamma - 1}$, which transforms the integral in Eq. (2.30) to

$$2\int_0^\infty dx\,\sqrt{2 + x^2}\ e^{-\rho(1+x^2)}\underset{\approx}{I}_l[p(x)]\ , \quad l\bar{\Omega} = 1\ . \tag{2.31}$$

In case 3, we divide the range of integration into two parts: a symmetric region about the singularity ($\gamma = l\bar{\Omega}$) and a part extending to infinity. Introducing a variable x such that $\gamma(x) = l\bar{\Omega} + (l\bar{\Omega} - 1)x$, integral in Eq. (2.30) becomes

$$\mathrm{P}\int_{-1}^{1} dx\,\frac{p(x)}{x}\,e^{-\rho\gamma(x)}\underset{\approx}{I}_l(x) + \int_{2l\bar{\Omega}-1}^\infty d\gamma\,\frac{pe^{-\rho\gamma}}{\gamma - l\bar{\Omega}}\underset{\approx}{I}_l[p(\gamma)]\ . \tag{2.32}$$

In the computations below with the relativistic dispersion relation, $\underset{\approx}{\sigma}^A$ is calculated from Eqs. (2.30)-(2.32).

Figure 3(a) shows the functional dependence of the $l = 1$ term (i.e., of the fundamental resonant term) of σ_{xx}^A on l and $\overline{\Omega}$ for fixed $n_\perp = 1.0$ and $n_z = 0$. Note that $n_\perp = 1.0$ is not the solution of the dispersion relation. At low temperature σ_{xx}^A follows almost exactly the cold plasma result,

$$\sigma_{xx}^{cold}(l = 1) = \frac{\omega_{pe}^2}{2\omega(\omega - |\Omega_e|)} .$$

The singularity at $\overline{\Omega} = 1$ dominates the wave propagation, absorption, and polarization in nonrelativistic theory, particularly for the extraordinary mode. We see in Fig. 3(a) that the resonance is washed out at high temperature and for $T \geq mc^2$ the $l = 1$ contribution converges to zero at all $\overline{\Omega}$. This does not imply that $\underset{\approx}{\sigma}^A$ itself is negligible at this temperature since higher l values must be included. Figure 3(b) shows $\sigma_{xx}^A(\overline{\Omega})$ total, including harmonics $-9 \leq l \leq 20$. At $T = 280$ keV this was necessary to achieve 1% accuracy in $\underset{\approx}{\sigma}^A$.

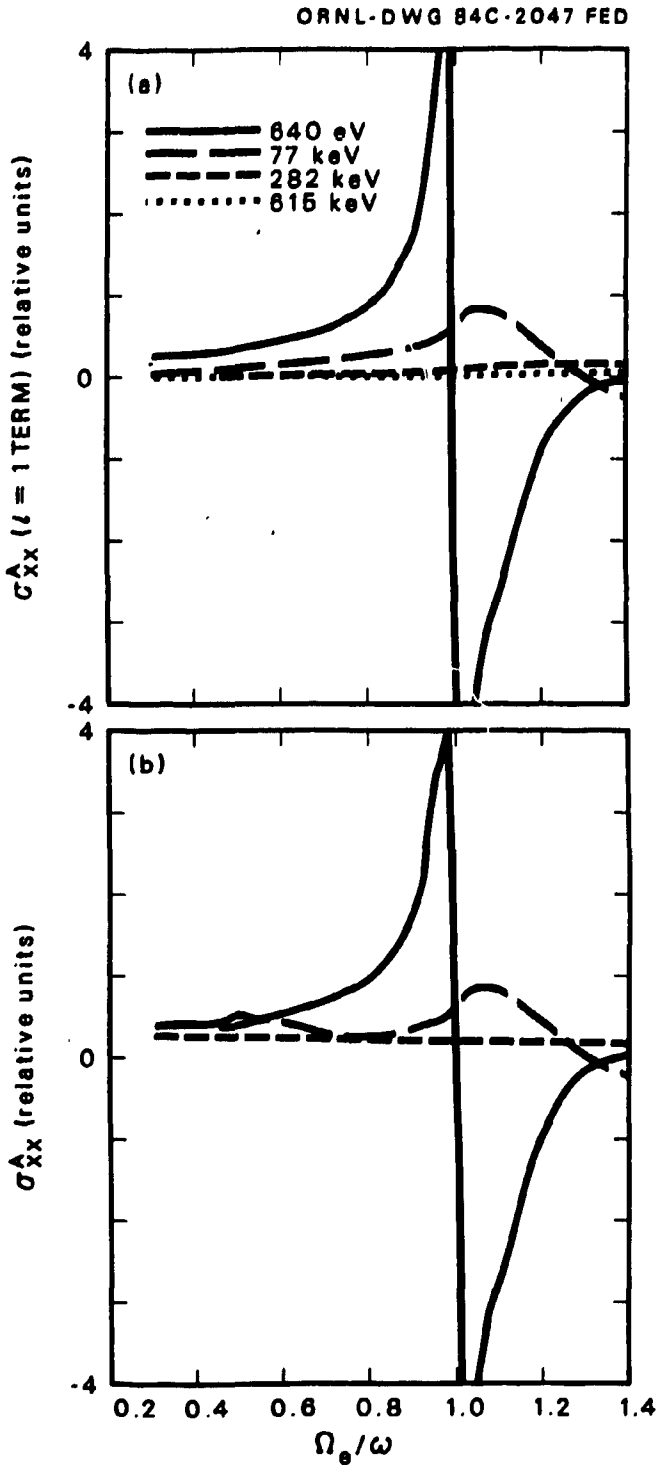

Fig. 3. Temperature dependence of $\sigma^A_{xx}(\Omega_e/\omega)$ for $n_z = 0$, $n_\perp = 1.0$. (a) $N = 1$ term, (b) sum of terms $N = -9$ through $N = 20$.

III. SOLUTION OF THE DISPERSION RELATION

In the limit $n_\parallel = 0$ the dispersion equation simplifies to

$$\begin{bmatrix} \epsilon_{xx} & \epsilon_{xy} & 0 \\ -\epsilon_{xy} & \epsilon_{yy} - n_\perp^2 & 0 \\ 0 & 0 & \epsilon_{zz} - n_\perp^2 \end{bmatrix} \begin{bmatrix} E_x \\ E_y \\ E_z \end{bmatrix} = 0 \ , \tag{3.1}$$

where $\underset{\approx}{\epsilon} = \underset{\approx}{I} + (4\pi i/\omega)\,(\underset{\approx}{\sigma}^A + \underset{\approx}{\sigma}^H)$. Also, the dispersion relation factors into ordinary and extraordinary mode branches,

$$n_\perp^2 - \epsilon_{zz}(n_\perp) = 0 : \text{ordinary mode} \ , \tag{3.2}$$

$$n_\perp^2 - \frac{\epsilon_{xx}(n_\perp)\epsilon_{yy}(n_\perp) - \epsilon_{xy}^2(n_\perp)}{\epsilon_{xx}(n_\perp)} = 0 : \text{extraordinary mode} \ . \tag{3.3}$$

These equations are solved numerically by standard root finding techniques.

Of course, the ϵ_{ij} are transcendental functions of $n_\perp$ so the dispersion relations have in general an infinite number of roots, including the electromagnetic ordinary and extraordinary modes as well as the Bernstein warm plasma modes. For simplicity, we first consider weakly damped modes ($n_i << n_r$) that go continuously into the electromagnetic waves at low temperature. This is accomplished by approximating $\underset{\approx}{\sigma}(n_{\perp r} + i n_{\perp i}) \simeq \underset{\approx}{\sigma}(n_{\perp r})$ and then solving Eqs. (3.2) and (3.3) for complex $n_\perp$, initializing the root finder to the appropriate cold plasma root. Figure 4 shows extraordinary mode k_r and k_i vs magnetic field strength (Ω_e/ω) for various values of T_e. For these calculations the wave frequency was $\omega/2\pi = 18$ GHz and the density was given by $\omega_{pe}^2/\omega^2 = 0.3$ (i.e., $n_e = 1.2 \times 10^{12}$ cm^{-3}). It should be mentioned that only the dimensionless quantities Ω_e/ω, ω_{pe}^2/ω^2, and T_e/mc^2 enter the dispersion relation for the refractive index $\underset{\sim}{n}$. The actual wave frequency therefore only enters as a scale factor on $\underset{\sim}{k} = \omega \underset{\sim}{n}/c$.

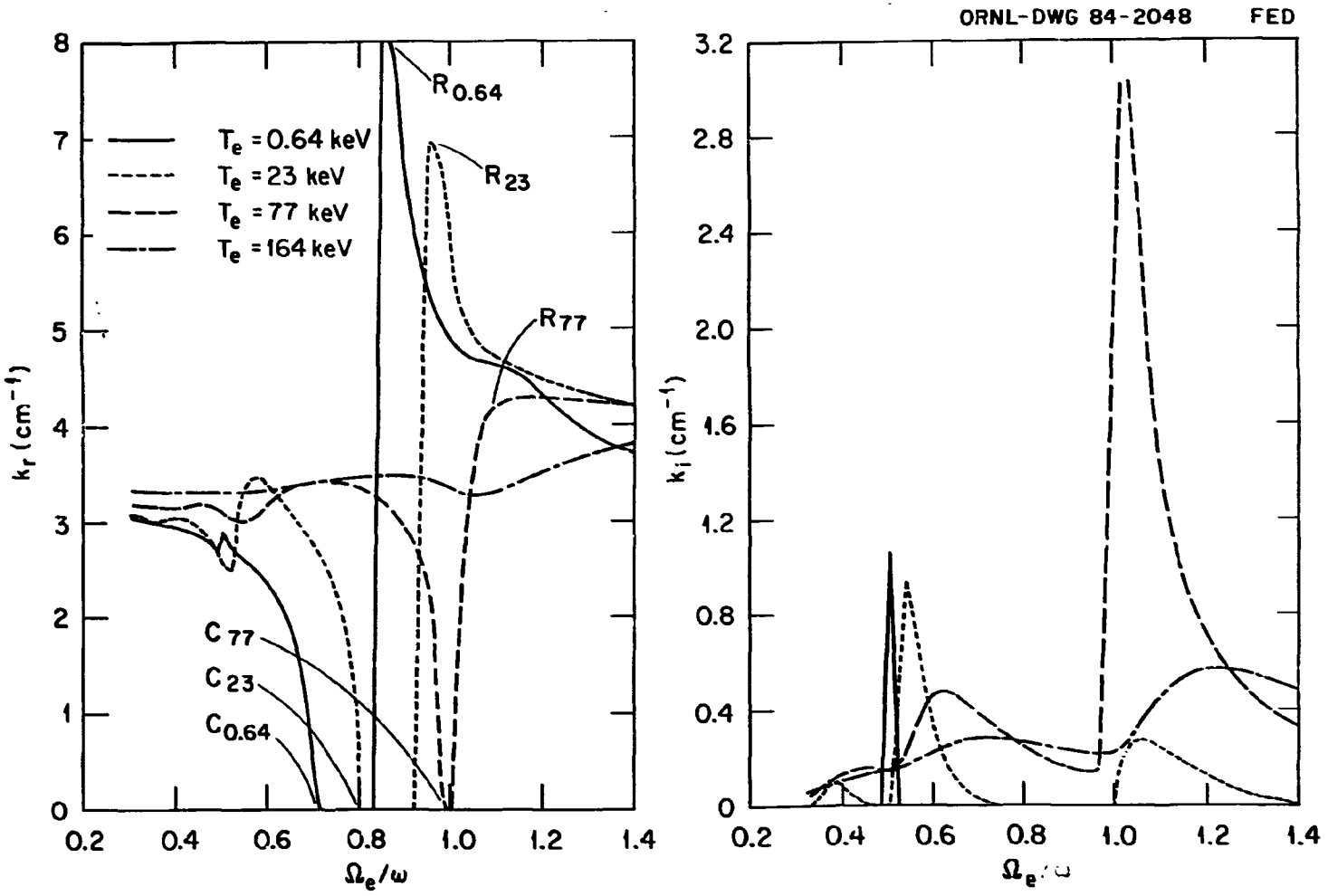

Fig. 4. Temperature dependence of (a) $k_r(\Omega_e/\omega)$ and (b) $k_i(\Omega_e/\omega)$ for $\omega/2\pi$ = 18 GHz, $\omega_{pe}^2/\omega^2 = 0.3$, $n_z = 0$. The argument of the Bessel functions was taken to be real.

At low temperature (T_e = 0.64 keV), k_r follows almost exactly the Appleton-Hartree solution except for a slight wiggle near the second harmonic (Ω_e/ω = 0.5) and a shoulder near the fundamental (Ω_e/ω = 1). In particular, the right-hand cutoff (denoted $C_{0.64}$ in the figure) and the upper hybrid resonance (denoted $R_{0.48}$) are at the correct cold plasma values. In Fig. 4(b) one sees a sharp second harmonic absorption line and invisibly small absorption at the fundamental. Recall that nonrelativistically, extraordinary mode, fundamental resonance absorption vanishes for $n_\parallel$ = 0. At higher temperature, T_e = 23 keV, one sees much larger and broader structure in k_r at the second harmonic and structure at the third harmonic. In k_i there are now broad peaks at the third harmonic and fundamental, whereas the second harmonic peak is reduced in size but greatly broadened. The most striking feature, however, is that the right-hand cutoff C_{23} and the upper hybrid resonance R_{23} have moved to higher magnetic field. Also, the maximum value of k_r at the resonance is only 7 cm^{-1}, which is about a factor of 2 above the free space value, k_0 = 3.77 cm^{-1}. At 77 keV the right-hand cutoff C_{77} and the upper hybrid resonance R_{77} have again moved to higher field but the cutoff has almost overtaken the resonance. There is virtually no maximum in k_r that would be associated with an upper hybrid resonance. Also note the general overlap of second and higher harmonics due to resonance broadening. At still higher temperature, T_e = 164 keV, the resonance/cutoff pair has disappeared altogether, leaving the merest vestige of cyclotron harmonic structure. The damping is relatively weak and nearly independent of magnetic field.

The interesting temperature dependence of the right-hand cutoff can be studied analytically using the dispersion relation. From Eqs. (3.2) and (3.3) we see that the condition for a true cutoff ($k_r = k_i = 0$) is

$$\epsilon_{zz}(n_\perp = 0) = 0 : \text{ordinary mode} ,$$

$$\epsilon_{xx}(n_\perp = 0)\epsilon_{xy}(n_\perp = 0) - \epsilon_{xy}^2(n_\perp = 0) = 0 : \text{extraordinary mode} . \tag{3.4}$$

In the limit $n_\perp \to 0$ for Eq. (2.27) the only nonzero terms are the $l = \pm 1$ terms of σ_{xx}, σ_{xy}, σ_{yy} and the $l = 0$ term of σ_{zz}. In particular, when $\bar{\Omega} < 1$, $\underset{\approx}{\sigma}^H = 0$, and we obtain for $\underset{\approx}{\epsilon}$

$$\epsilon_{xx} = \epsilon_{yy} = 1 - \frac{\omega_{pe}^2}{\omega^2}\frac{p^2}{3K_2(\rho)}\int_0^\infty dp \frac{p^4 e^{-p\gamma}}{p^2 + 1 - \bar{\Omega}^2} , \tag{3.5}$$

$$\epsilon_{xy} = i\bar{\Omega}\,\frac{\omega_{pe}^2}{\omega^2}\,\frac{\rho^2}{3K_2(\rho)}\int_0^\infty dp\,\frac{p^4 e^{-\rho\gamma}}{\gamma(p^2+1-\bar{\Omega}^2)}\ , \tag{3.6}$$

$$\epsilon_{zz} = 1 - \frac{\omega_{pe}^2}{\omega^2}\,\frac{\rho^2}{3K_2(\rho)}\int_0^\infty dp\,\frac{p^4}{\gamma^2}e^{-\rho\gamma}\ . \tag{3.7}$$

Equation (3.6) can be solved immediately to give the density of the ordinary mod cutoff,

$$\left(\frac{\omega_{pe}^2}{\omega^2}\right)_{cutoff} = \frac{3K_2(\rho)}{\rho^2\int_0^\infty dp\ \frac{p^4}{\gamma^2}e^{-\rho\gamma}}\ . \tag{3.8}$$

The right-hand side of Eq. (3.8) is an increasing function of temperature, which i the nonrelativistic limit ($\rho \gg 1$) approaches unity.

Equations (3.5) and (3.6) can also be used to derive an expression for th magnetic field of the right-hand cutoff. However, the integrals cannot be performe analytically, so in Fig. 5 we have plotted $(\Omega_e/\omega)_{cutoff}$ vs temperature for variou densities, Ω_{pe}^2/ω^2. The curves terminate when $\Omega_e/\omega = 1$. This is because $\underset{\approx}{\sigma}^H$ nonzero for $\Omega_e/\omega > 1$, and the cutoff condition becomes complex. Both the re and imaginary parts of Eq. (3.4) cannot be made to vanish simultaneously for re Ω_e/ω. Thus in Fig. 4 and in the figures to follow, as increasing temperatu attempts to push $(\Omega_e/\omega)_{cutoff}$ beyond unity, the cutoff disappears altogether. No that the location of the cutoff in Fig. 4 is accurately given by Eqs. (3.4)-(3.6).

The calculations above show in a simple way the trends with increasing ten perature. However, because n_i was neglected in $\underset{\approx}{\sigma}$, the results are not accura near the cutoff $k_r \to 0$ in the evanescent region nor for the $T_e = 77$ keV ca near the fundamental, where the damping is strong. We remedy this now by allov ing a complex argument for $\underset{\approx}{\sigma}$. This allows us to study heavily damped ar evanescent waves and introduces the Bernstein mode roots. We will see that t coupling between the extraordinary and Bernstein modes is quite interesting a complicated, particularly in the region of magnetic field strength between the c plasma extraordinary mode cutoff, $\Omega_e/\omega = 1 - \omega_{pe}^2/\omega^2$, and the fundamen cyclotron resonance.

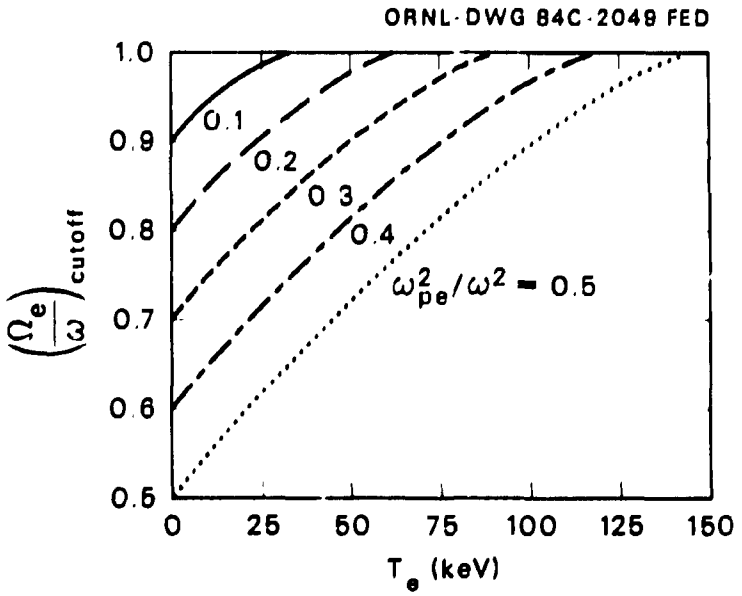

Fig. 5. Magnetic field strength for right-hand cutoff vs temperature for various values of ω_{pe}^2/ω^2.

The behavior of extraordinary and Bernstein mode roots has been investigated rather thoroughly in the weakly relativistic limit near the second harmonic resonance.[11,12] In that work a critical density was identified that for fixed temperature separates two regimes with different connection properties of the mode across the second harmonic [see, for example, Eq. (10) and following material of Ref. 11]. We consider first a case corresponding to the low density regime of the weakly relativistic theory.

Figure 6 shows k_r (solid lines) and k_i (dashed lines) of the extraordinary and Bernstein modes as functions of Ω_e/ω for temperatures of (a) 16 keV, (b) 52 keV, (c) 77 keV, and (d) 185 keV. The wave frequency is $\omega = 2\pi \times 18$ GHz, and the plasma density is given by $\omega_{pe}^2/\omega^2 = 0.2$. For $T_e = 16$ keV the extraordinary mode is continuous through the second harmonic resonance with a perturbation near $\Omega_e/\omega = 0.5$ due to the intersection of the Bernstein mode. The location of the right-hand cutoff has been displaced by relativistic effects from the cold plasma value of $\Omega_e/\omega = 0.7$ up to 0.87, while the maximum of k_r on the extraordinary mode branch occurs at $\Omega_e/\omega = 0.96$ rather than 0.84, which is the upper hybrid resonance. This plot is comparable to Fig. 1 of Ref. 11 (note, however, that the ordinate in that plot is ω/Ω_e rather than Ω_e/ω, and it does not show the

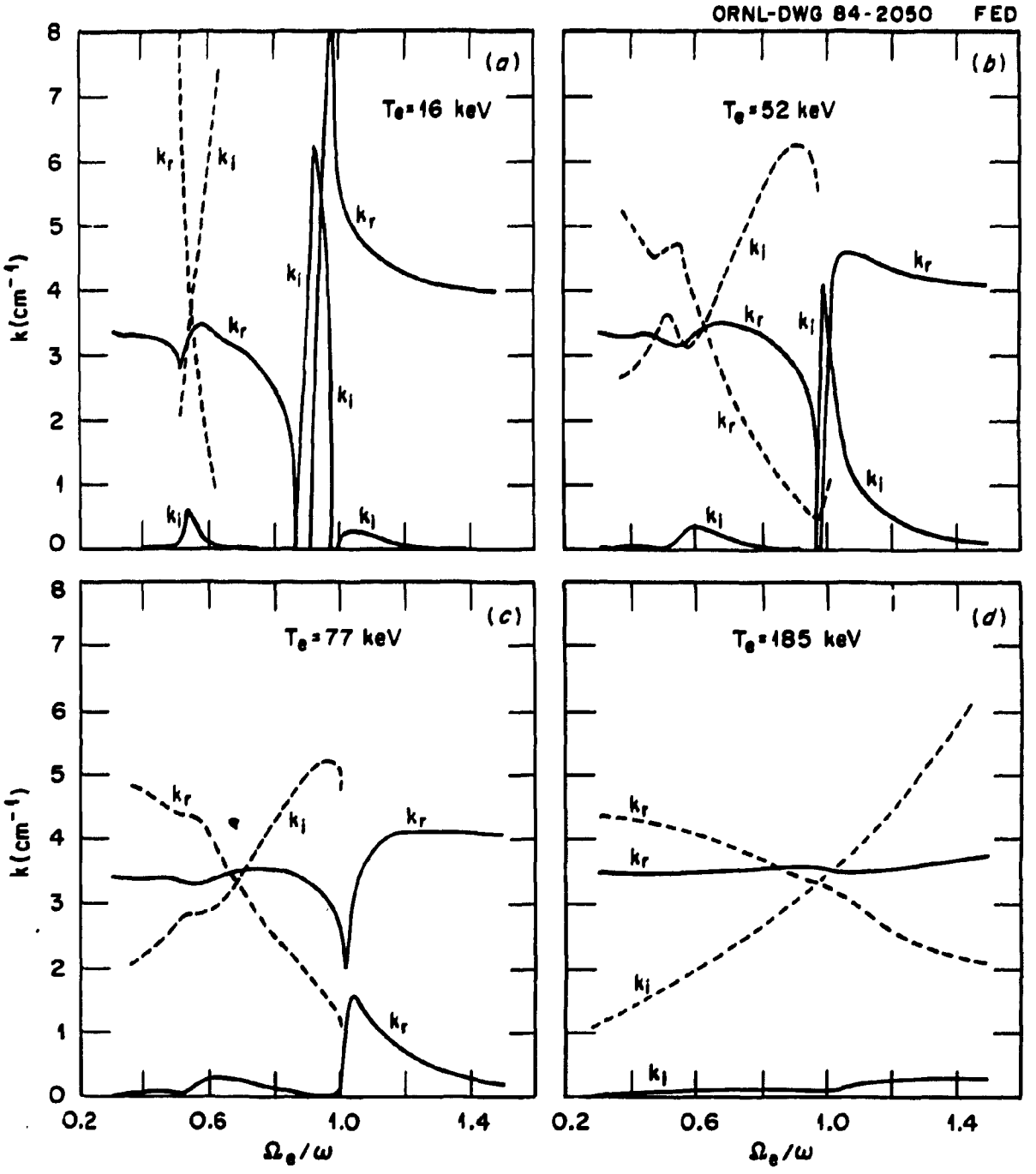

Fig. 6. $k_r(\Omega_e/\omega)$ and $k_j(\Omega_e/\omega)$ for the extraordinary mode branch (solid lines) and Bernstein mode branch (dashed lines) with $\omega_{pe}^2/\omega^2 = 0.2$, $n_\parallel = 0$ for (a) $T_e = 16$ keV, (b) $T_e = 52$ keV, (c) $T_e = 77$ keV, and (d) $T_e = 185$ keV.

Bernstein mode). As the temperature is increased to 52 keV [Fig. 6(b)], the right-hand cutoff moves to $\Omega_e/\omega = 0.98$ and virtually all peaking in k_r that would be associated with the upper hybrid is gone. Additional structure is seen in the Bernstein mode near the second harmonic resonance. At higher temperature the cutoff attempts to move above $\Omega_e/\omega = 1.0$ and the resonance/cutoff pair effectively annihilate each other. According to Fig. 5 the critical temperature for $\omega_{pe}^2/\omega^2 = 0.2$ is 62 keV. In Fig. 6(c), $T_e = 77$ keV, there is no cutoff at any magnetic field for the extraordinary mode, although damping is quite strong near the fundamental. At very high temperature, $T_e = 185$ keV in Fig. 6(d), k_r for the extraordinary mode is almost independent of magnetic field with only a slight perturbation due to the presence of the Bernstein mode. The damping is weak and almost all harmonic structure is washed out.

In Fig. 6(a and b) we have not plotted the Bernstein mode root for $\bar{\Omega} > 1$. The Hermitian part of the conductivity is not an analytic function of Ω_e at $\bar{\Omega} = 1$ because of the factor $p_+ = (\lambda^2\bar{\Omega}^2 - 1)^{1/2}$ in Eq. (2.24). At these intermediate temperatures the magnitude of $k_\perp$ for the Bernstein mode is large and the $l = 1$ contribution to σ^H turns on, very rapidly making the roots difficult to follow numerically. The Bernstein mode itself is strongly damped here and of little practical importance. It is interesting, however, to see how this mode influences the extraordinary mode root near the fundamental resonance. We will defer this topic for future publications.

In the weakly relativistic theory, as the density is increased, a regime is reached in which the Bernstein mode on the low magnetic field side joins smoothly onto the extraordinary mode above the second harmonic resonance. Figure 7 shows such a high density regime case, $\omega_{pe}^2/\omega^2 = 0.3$, for temperatures of (a) 16 keV, (b) 52 keV, (c) 108 keV, and (d) 185 keV. In Fig. 7(a), $T_e = 16$ keV, we see that the extraordinary mode from the low field side joins a heavily damped mode at the second harmonic resonance (denoted AB in the figure). As previously mentioned, the Bernstein mode connects to the extraordinary mode branch above the second harmonic (point C). With increasing Ω_e/ω the extraordinary mode continues to the cutoff (accurately predicted by Fig. 5) and joins to the evanescent extraordinary mode point D coming from the high field side of the fundamental. The extraordinary mode therefore exists as two disconnected branches with a break at AC. Now, as the temperature is increased, k_r increases for the heavily damped mode (AB), approaching the Bernstein mode at $\Omega_e/\omega \simeq 0.5$ and approaching the evanescent extraordinary mode near the right-hand cutoff. In Fig. 7(b), $T_e =$

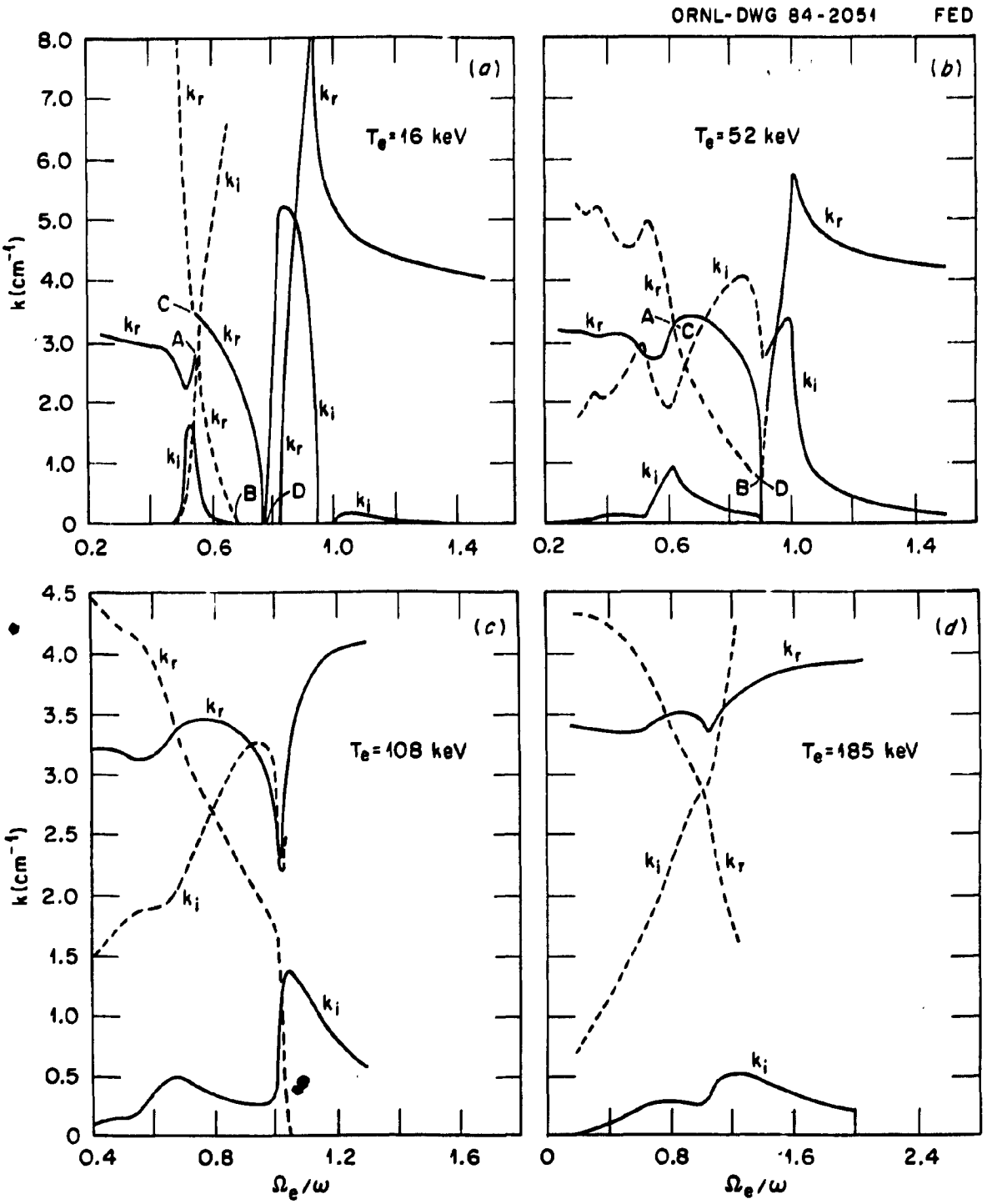

Fig. 7. $k_r(\Omega_e/\omega)$ and $k_i(\Omega_e/\omega)$ for the extraordinary mode branch (solid lines) end Bernstein mode branch (dashed lines) with $\omega_{pe}^2/\omega^2 = 0.3$, $n_\parallel = 0$ for (a) $T_e = 16$ keV, (b) $T_e = 52$ keV, (c) $T_e = 108$ keV, and (d) $T_e = 185$ keV.

52 keV, the heavily damped mode has joined the Bernstein mode, while the extraordinary mode on the low field side is continuous with the branch of the extraordinary mode that goes to the cutoff (point D). That is, point A now coincides with point C. The weakly damped mode joins smoothly with the extraordinary mode coming from the high field side at point B. Again the extraordinary mode is in two disconnected branches, but this time the break is at BD. As the temperature is increased to 108 keV, Fig. 7(c), the cutoff disappears and the extraordinary mode again becomes a single continuous branch. The Bernstein mode makes only a minor perturbation at the second harmonic but strongly influences the extraordinary mode near the fundamental. At $T_e = 185$ keV, Fig. 7(d), the extraordinary mode is smooth and weakly damped throughout.

Solution of Eq. (3.2) for the ordinary mode can be carried out in the same manner. Of primary interest here is the dependence of k on density. Figure 8 shows k_r vs ω_{pe}^2/ω^2 for temperatures of 0.9 keV, 24 keV, and 78 keV. At low temperatures k_r follows the cold plasma results, $1 - \omega_{pe}^2/\omega^2$, quite closely. Increasing temperature increases k_r at fixed ω_{pe}^2/ω^2 toward the vacuum value $k_0 = 3.77\ \text{cm}^{-1}$ and also increases the density of the cutoff. Again the cutoff density is accurately given by Eq. (3.8).

It is also of interest to examine the effects of high temperature on the electric field polarization eigenvectors, that is, the solution of Eq. (3.1). In cold plasma theory the singularity of $\underset{\approx}{\sigma}^A$ at $\omega = \Omega_e$ completely "shields out" the right circularly polarized component of the field, $E_- = E_x - iE_y$, at the fundamental resonance. If $n_\parallel \neq 0$, even nonrelativistically finite temperature effects resolve the singularity and allow a small component of E_- at the fundamental resonance. This small correction to $\underset{\sim}{E}$ is quite important for calculation of cyclotron damping at the fundamental using the Poynting theorem (see, for example, Ref. 13) although away from the fundamental the cold plasma eigenvectors can be used. Figure 9 shows the magnitude of the E_- component for the extraordinary mode vs Ω_e/ω for temperature $T = 2.5$ keV, 23 keV, and 64 keV. The wave frequency is 18 GHz and the plasma density is $\omega_{pe}^2/\omega^2 = 0.3$. The total eigenvector has been normalized such that $\underset{\sim}{E}^* \cdot \underset{\sim}{E} = 1$. We see the dip in $|E_-|$ at $\Omega_e/\omega \simeq 1$ for the low temperatures, but this is completely gone at higher temperature.

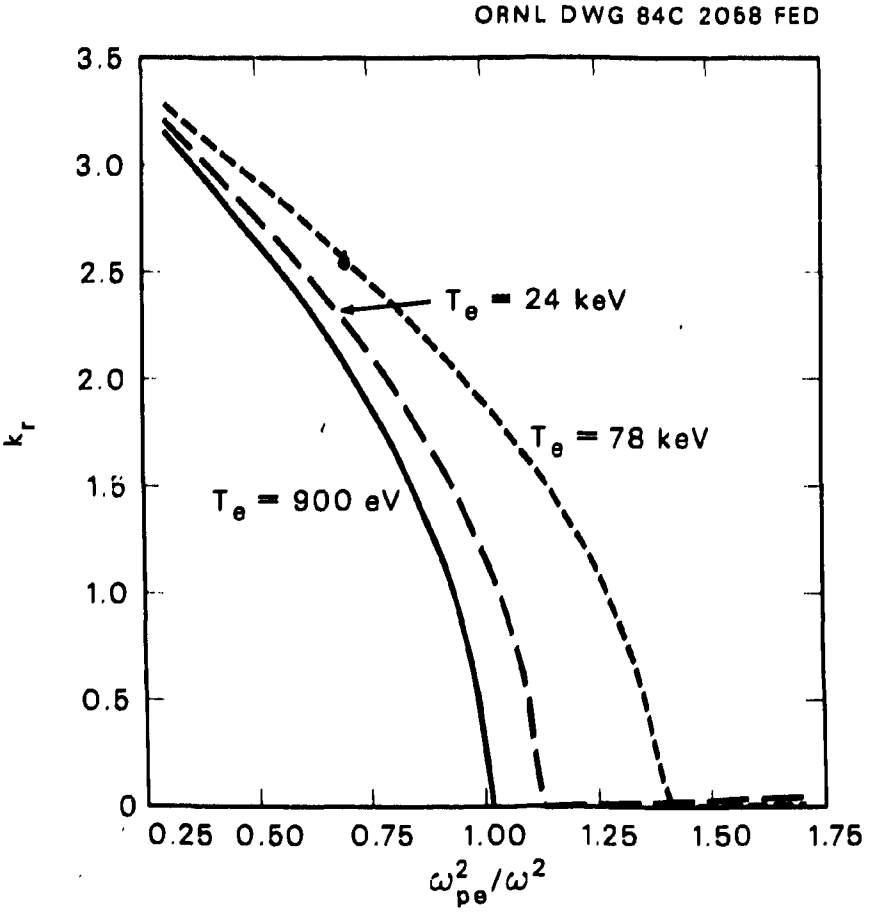

Fig. 8. k_r vs ω_{pe}^2/ω^2 for T_e = 0.9 keV, 24 keV, and 78 keV.

IV. COMPARISON WITH POYNTING THEOREM CALCULATIONS

One of our main objectives has been to determine how well the Poynting theorem model [Eq. (1)] using cold plasma values of $\underset{\sim}{k}_r$ and $\underset{\sim}{E}$ agrees with the solutions of the full dispersion relation. Figure 10 compares k_l obtained from the dispersion relation (solid curve) with k_l obtained from the Poynting theorem (dashed curve) for temperatures of (a) 52 keV, (b) 185 keV, and (c) 1 MeV. The wave frequency is again 18 GHz, and the plasma density is 1.2×10^{12} cm^{-2} ($\omega_{pe}^2/\omega^2 = 0.3$). Since the waves are relatively weakly damped, for ease in computations at the very high temperatures we have employed the version of the code using real arguments for the Bessel function (this code was used to produce Fig. 4). It is clear that the Poynting model must fail at the cold plasma cutoff ($\Omega_e/\omega = 0.7$ in Fig. 10). Since the cold plasma k_r vanishes there, all the Bessel functions in $\underset{\approx}{\sigma}^H$

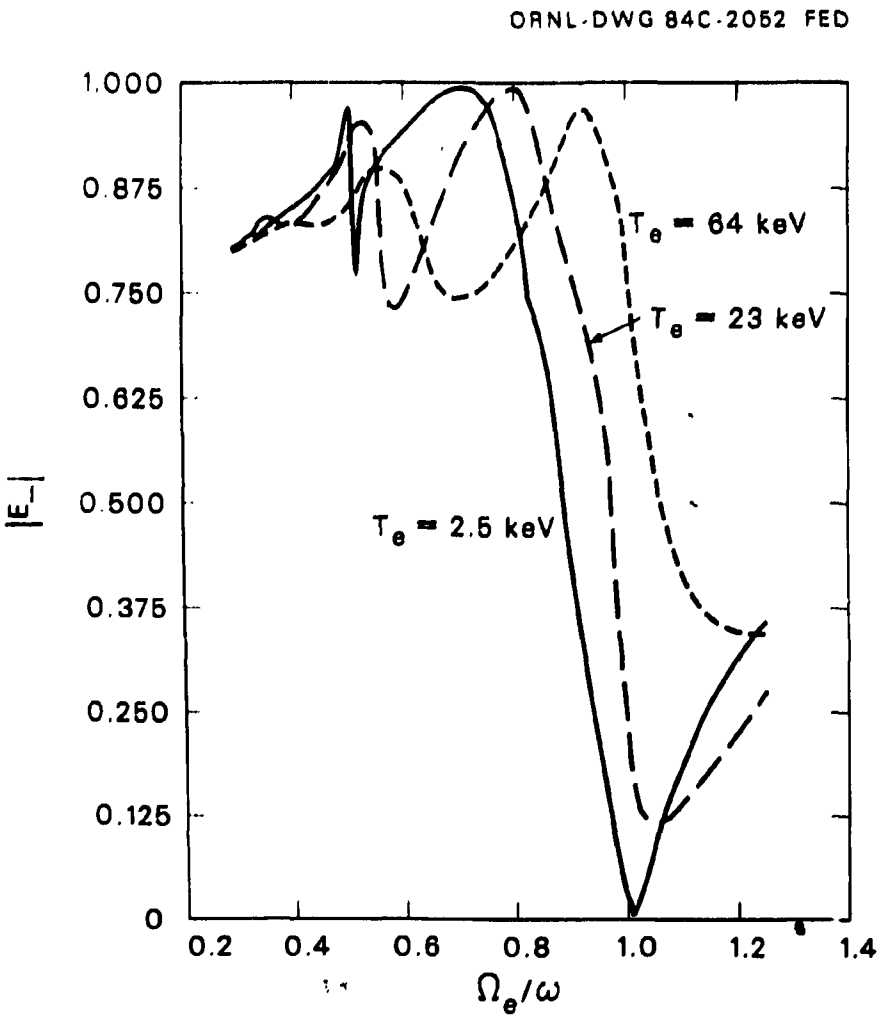

Fig. 9. Right circularly polarized component of extraordinary mode $\underset{\sim}{E}$ (i.e., $|E_-|/|\underset{\sim}{E}|$) vs Ω_e/ω for various temperatures.

are zero, resulting in zero absorption. The Poynting theorem results are not meaningful between the cutoff and fundamental resonance because the cold plasma root is purely evanescent. On the other hand, with the full dispersion relation, neither k_r nor k_i vanishes at the cold plasma cutoff. Similarly, the Poynting model must fail near $\Omega_e/\omega = 1$ since in cold plasma theory E_- is zero at the fundamental, whereas relativistically $E_-/|E|$ is of order one. From Fig. 10 we see that at the second and higher harmonics (i.e., $\Omega_e/\omega \leq 0.5$) the Poynting theorem calcu .tion is reasonably accurate up to 185 keV. Notice that the absorption predicted by the

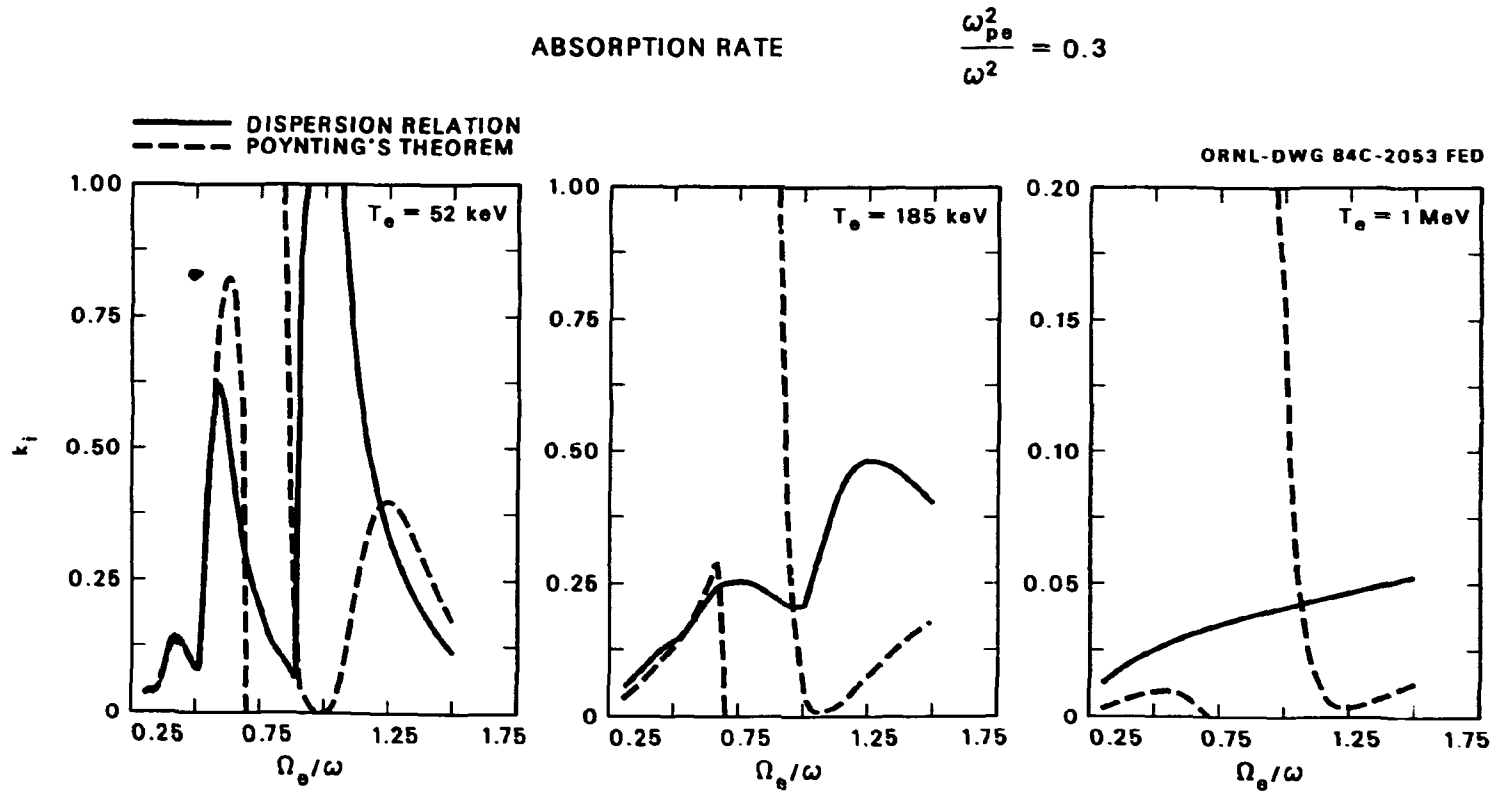

Fig. 10. Comparison between $k_i(\Omega_e/\omega)$ obtained from the dispersion relation (solid line) and $k_i(\Omega_e/\omega)$ obtained from the Poynting theorem (dashed line) in a purely hot plasma with $\omega_{pe}^2 = 0.3$ at (a) $T_e = 50$ keV, (b) $T_e = 185$ keV, and (c) $T_e = 1$ MeV.

Poynting theorem is nonzero at $\Omega_e/\omega = 1$. This is the contribution due to the left circularly polarized component, E_+, which becomes significant at high temperature.

The justification for using the Poynting theorem code for EBT calculations was that the hot plasma in EBT is coexistent with a much cooler component with higher density [$T_{cold} \sim 300$ eV, $n_{cold} \sim (2\text{-}10)n_{hot}$]. It was considered that k_r and $\underset{\sim}{E}$ would be dominated by the cold component, which would render the Poynting theorem formulation valid for EBT even in the range 0.5-1 MeV. We have therefore investigated the effect of adding a cold component in both formulations. In Fig. 11 we compare absorption calculations in which the total plasma density is 1.2×10^{12} cm^{-3} ($\omega_{pe}^2/\omega^2 = 0.3$) with the hot component ($T_e = 502$ keV) representing all of the density, Fig. 11(a); only half of the density [$(\omega_{pe}^2/\omega^2)_{hot} = 0.15$], Fig. 11(b); and one-sixth of the density [$(\omega_{pe}^2/\omega^2)_{hot} = 0.05$], Fig. 11(c).

The remainder of the plasma is described by the purely anti-Hermitian, cold plasma conductivity. One can see that the agreement is significantly better than for the comparable case of purely hot plasma [Fig. 11(a)]. The presence of the cold plasma component effectively shields out the E_- component of the wave field and results in reduced absorption and much improved agreement between models at the fundamental resonance. It is interesting that the presence of the cold plasma component reintroduces the right-hand cutoff in the calculations with the full dispersion relation, although the hot plasma component shifts the cutoff to a higher magnetic field than the cold plasma value. We have not plotted k_r here, but the zeros in k_i above the second harmonic in Fig. 11 are in fact associated with the cutoff.

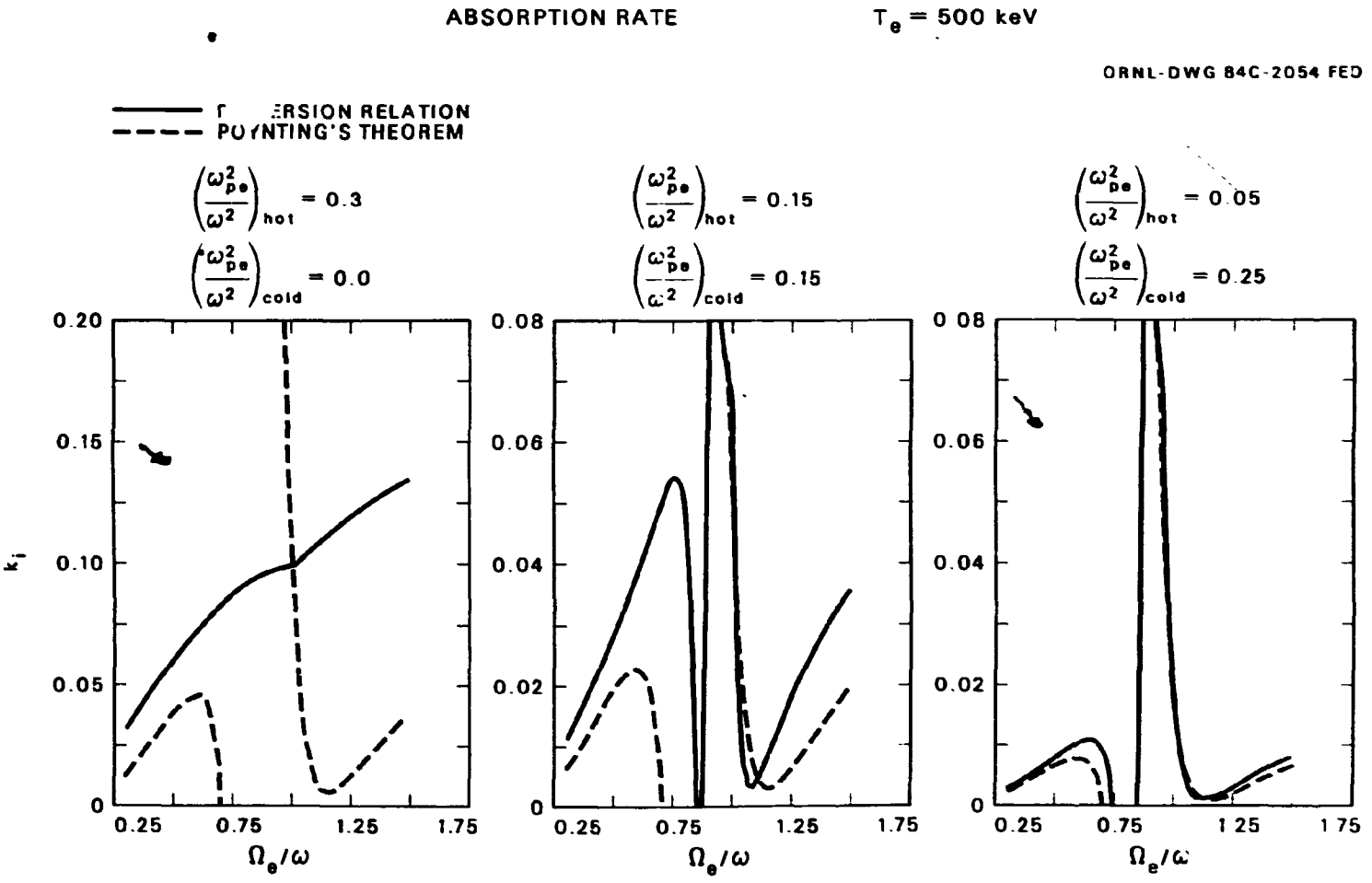

Fig. 11. Comparison between $k_i(\Omega_e/\omega)$ obtained from the dispersion relation (solid line) and $k_i(\Omega_e/\omega)$ obtained from the Poynting theorem (dashed line) in superposition of hot and cold plasma components. Here $T_e = 500$ keV, $n_z = 0.0$, $(\omega_{pe}^2/\omega^2)_{total} = 0.3$, and (a) $(\omega_{pe}^2/\omega^2)_{hot} = 0.3$, $(\omega_{pe}^2/\omega^2)_{cold} = 0.0$; (b) $(\omega_{pe}^2/\omega^2)_{hot} = 0.15$, $(\omega_{pe}^2/\omega^2)_{cold} = 0.15$; (c) $(\omega_{pe}^2/\omega^2)_{hot} = 0.05$, $(\omega_{pe}^2/\omega^2)_{cold} = 0.25$.

V. CONCLUSIONS

We have found that for $n_\parallel = 0$ and T_e above a few tens of kilo-electron-volts both the wave number, k_r ($\simeq \underset{\approx}{\sigma}^A$), and damping rate, k_i ($\simeq \underset{\approx}{\sigma}^H$), are significantly modified by relativistic mass shift and large $k_\perp \rho_e$. Above about 40 keV, cyclotron harmonic overlap becomes important and at least three harmonics must be included. To obtain 1% accuracy in calculating σ^A at 280 keV [Fig. 3(b)] it was necessary to include harmonics $l = -9$ to $l = 20$.

As one would expect intuitively, the relativistic mass increase associated with increasing T_e reduces the dispersive property of the plasma. Both the right-hand cutoff and the upper hybrid resonance move to higher magnetic field and the separation between them decreases. At sufficiently high temperature (see Fig. 5) the resonance and cutoff disappear altogether. Above this temperature the extraordinary mode has no evanescent region, $k_r = 0$, at any magnetic field. Above about 20 keV there are significant deviations in k_r from the cold plasma value. Of course, the discrepancy is most pronounced near the cutoff and upper hybrid resonance, but large differences occur throughout the range $0.5 \leqslant \Omega_e/\omega \leqslant 1.5$. As T_e increases, the cyclotron harmonic structure washes out due to resonance overlap and the magnitude of $\underset{\approx}{\sigma}^A$ decreases. Thus for $T_e > m_e c^2$, k_r approaches the vacuum value, $k_r = \omega/c$.

These results have interesting consequences for ray tracing. Over most of parameter space the cold plasma rays should be valid when $T_e < 10$-20 keV. Also, for $T_e > 500$ keV, plasma dispersion can be neglected and straight-line vacuum trajectories used. There is, however, an uncomfortable range, 20 keV $\leqslant T_e \leqslant$ 500 keV, in which electromagnetic waves can be weakly damped, but the ray trajectories are not well described by either cold plasma theory or vacuum solutions. An additional complication comes in through the temperature dependence of k_r, which may result in ray refraction due to temperature gradients.

For temperatures less than about 20 keV, our calculations are in relatively good agreement with the weakly relativistic expansion of Shkarofsky.[3] Much above this temperature resonance overlap becomes important, the expansion of γ breaks down, and the small Larmor radius expansion of the Bessel function is not valid. From the standpoint of heating hot electron plasmas, one of the most important features we have observed is that for fixed Ω_e/ω the absorption rate, k_i, peaks at a certain finite temperature, then decreases above this point. At the second harmonic resonance, the peak absorption occurs at $T_e = 75$ keV. For $T_e > 500$ keV, k_i is

approximately proportional to $T_e^{-3/2}$, which is the asymptotic behavior of the normalization factor of the relativistic Maxwellian, $e/K_2(\rho)$. This effect can be understood physically as follows: cyclotron harmonic absorption is a finite Larmor radius effect, $k_l \sim \langle J_l^2 (k_{\perp r} v_\perp/\Omega)\rangle$, so that at low temperature k_l increases with $\langle v_\perp \rangle$. However, at high temperatures the distribution is widely spread out in velocity space so that the density of particles resonant with a wave of fixed $(\underset{\sim}{k}, \omega)$ decreases as temperature increases. As a practical matter, our calculations have shown that due to higher ring temperature in EBT-S ($T_{ring} \sim$ 400-500 keV) compared to EBT-I ($T_{ring} \sim$ 150-200 keV), less power is actually deposited in EBT-S rings despite the much higher ring stored energy (typically 30-40 J compared to 5-10 J in EBT-I). In advanced devices using still higher ring temperatures ($T_{ring} \sim$ 1 MeV projected for the EBT-P device), methods of efficiently coupling power to the hot electrons are an important consideration.[9] These results also point out the sensitivity of absorption to details of the distribution function, particularly deviations from a simple Maxwellian.

We are encouraged by the agreement between calculations with the full dispersion relation and the Poynting theorem using cold plasma k_r and $\underset{\sim}{E}$. In circumstances for which the relativistic plasma component is embedded in a nonrelativistic component of equal or higher density, the Poynting theorem formulation gives reasonably accurate results to well above 500 keV. This is much less demanding computationally than solving the full dispersion relation. We feel, therefore, that within the limits of WKB theory, our previous calculations of EBT ring absorption are correct. There are, of course, uncertainties as to whether any WKB-like theory can be applied to the EBT rings, where the perpendicular magnetic field scale length is not much greater than ρ and where particles with $v_\parallel \sim c$ see variations in magnetic field strength in a few gyroperiods by parallel flow.

Figures 6 and 7 demonstrate the complicated interaction between the extraordinary mode and the Bernstein mode at high temperature. Since both modes tend to be heavily damped near the coupling point it is not clear that these couplings are important for practical applications at relativistic temperatures. In any case, accurate computation of mode conversion requires a full wave treatment, which in this large $k_\perp \rho_e$ regime would be extremely difficult.

Finally, we should comment on the computational requirements. Some effort has been expended in making the computation of Bessel functions and the numerical integrations run efficiently. Despite this effort, the code is quite expensive to run. This has discouraged us from investigating more general distribution functions or a

wider parameter space (e.g., $n_\parallel \neq 0$). There are, however, other formulations for the relativistic conductivity tensor that may have computational advantages over the cyclotron harmonic expansion used here. In particular, there is Trubnikov's original formulation mentioned in the introduction. Also, a formulation by Weitzner[14] exists in which the sum over cyclotron harmonics is replaced by an integral over the order of a combination of Bessel functions.

REFERENCES

1. B. A. Trubnikov, in *Plasma Physics and the Problem of Controlled The monuclear Reactions*, edited by M. A. Leontovich (Pergamon Press, Inc New York, 1959), Vol. III, p. 122.
2. Y. N. Dnestrovskii, D. P. Kostomarov, and N. V. Skrydlov, Sov. Phy Tech. Phys. **8**, 691 (1964).
3. I. P. Shkarofsky, Phys. Fluids **9**, 561 (1966); Phys. Fluids **9**, 570 (1966).
4. K. R. Chu and B. Hui, Phys. Fluids **26**, 69 (1983).
5. K. Imre and H. Weitzner, "Relativistic Broadening Near Cyclotron Res nance," Courant Institute of Mathematical Sciences Report MF-101, Octob 1983.
6. M. Bornatici, R. Cano, O. DeBarbieri, and F. Engelman, Nucl. Fusion **2** 1153 (1983).
7. N. A. Uckan, Phys. Fluids **25**, 2381 (1982).
8. D. E. Baldwin and B. G. Logan, "Physics Basis for an Axicell Design f the End Plugs of MFTF-B," Lawrence Livermore National Laboratory Repc UCID-19359, April 1982.
9. D. B. Batchelor, R. C. Goldfinger, and D. A. Rasmussen, Oak Rid National Laboratory Report ORNL/TM-8770, 1983 (to be published in Ph sics of Fluids).
10. S. Tamor, Nucl. Fusion **18**, 229 (1978).
11. M. Bornatici, F. Engelmann, C. Maroli, and V. Petrillo, Plasma Phys. **2** 89 (1981).
12. E. Lazzaro and G. Ramponi, Plasma Phys. **23**, 53 (1981).
13. H. Weitzner and D. B. Batchelor, Phys. Fluids **23**, 1359 (1980).
14. I. Weiss and H. Weitzner, "Electromagnetic Wave Propagation in Relativis Magnetized Plasmas," to be published.

ORNL/TM-9075
Dist. Category UC-20 f,g

INTERNAL DISTRIBUTION

1. F. W.Baity
2-11. D. B. Batchelor
12. R. J. Colchin
13. W. A. Cooper
14. W. A. Davis
15. R. A. Dory
16. J. L. Dunlap
17. S. A. Freije
18. J. C. Glowienka
19-24. R. C. Goldfinger
25. G. R. Haste
26. D. L. Hillis
27. M. J. Saltmarsh
28. J. Sheffield
29. D. A. Spong
30. T. Tucker
31. N. A. Uckan
32-33. Laboratory Records Department
34. Laboratory Records, ORNL-RC
35. Document Reference Section
36. Central Research Library
37. Fusion Energy Division Library
38. Fusion Energy Division Reports Office
39. ORNL Patent Office

EXTERNAL DISTRIBUTION

40. Office of the Assistant Manager for Energy Research and Development, Department of Energy, Oak Ridge Operations Office, P.O.Box E, Oak Ridge, TN 37831
41. J. D. Callen, Department of Nuclear Engineering, University of Wisconsin, Madison, WI 53706
42. S. O. Dean, Fusion Power Associates, 2 Professional Drive, Suite 248, Gaithersburg, MD 20879
43. H. K. Forsen, Bechtel Group, Inc., Research Engineering, P. O. Box 3965, San Francisco, CA 94205
44. R. W. Gould, Department of Applied Physics, California Institute of Technology, Pasadena, CA 91125
45. D. G. McAlees, Exxon Nuclear Co., Inc., 777 106th Avenue, NE, Bellevue, WA 98349
46. P. J. Reardon, Brookhaven National Laboratory, Upton, NY 11973
47. W. M. Stacey, School of Nuclear Engineering, Georgia Institute of Technology, Atlanta, GA 30332
48. G. A. Eliseev, I. V. Kurchatov Institute of Atomic Energy, P.O. Box 3402, 123182 Moscow, U.S.S.R.

49. V. A. Glukhikh, Scientific-Research Institute of Electro-Physical Apparatus, 188631 Leningrad, U.S.S.R.
50. I. Spighel, Lebedev Physical Institute, Leninsky Prospect 53, 117924 Moscow, U.S.S.R.
51. D. D. Ryutov, Institute of Nuclear Physics, Siberian Branch of the Academy of Sciences of the U.S.S.R., Sovetskaya St. 5, 630090 Novosibirsk, U.S.S.R.
52. V. T. Tolok, Kharkov Physical-Technical Institute, Academical St. 1, 310108 Kharkov, U.S.S.R.
53. R. Varma, Physical Research Laboratory, Navrangpura, Ahmedabad 384209, India
54. Bibliothek, Max-Planck Institut fur Plasmaphysik, D-8046 Garching bei Munchen, Federal Republic of Germany
55. Bibliothek, Institut fur Plasmaphysik, KFA, Postfach 1913, D-5170 Julich, Federal Republic of Germany
56. Bibliotheque, Centre des Recherches en Physique des Plasmas, 21 Avenue des Bains, 1007 Lausanne, Switzerland
57. Bibliotheque, Service du Confinement des Plasmas, CEA, B.P. No. 6, 92 Fontenay-aux-Roses (Seine), France
58. Documentation S.I.G.N., Departement de la Physique du Plasma et de la Fusion Controlee, Centre d'Etudes Nucleaires, B.P. 85, Centre du Tri, 38081 Cedex, Grenoble, France
59. Library, Culham Laboratory, UKAEA, Abingdon, Oxon, OX14 3DB, England
60. Library, FOM-Instituut voor Plasma-Fysica, Rijnhuizen, Jutphaas, The Netherlands
61. Library, Institute of Physics, Academia Sinica, Beijing, Peoples Republic of China
62. Library, Institute of Plasma Physics, Nagoya University, Nagoya, Japan
63. Library, International Centre for Theoretical Physics, Trieste, Italy
64. Library, Laboratorio Gas Ionizatti, Frascati, Italy
65. Library, Plasma Physics Laboratory, Kyoto University, Gokasho Uji, Kyoto, Japan
66. Plasma Research Laboratory, Australian National University, P.O. Box 4, Canberra, A.C.T. 2000, Australia
67. Thermonuclear Library, Japan Atomic Energy Research Institute, Tokai, Naka, Ibaraki, Japan
68. W. Ard, McDonnell Douglas Astronautics Company, P.O. Box 516, St. Louis, MO 63166
69. K. Audernaerde, Nuclear Engineering Department, University of Wisconsin, 1500 Johnson Drive, Madison, WI 53706
96.70. M. Azumi, Division of Thermonuclear Research, Japan Atomic Energy Research Institute, Tokai, Ibaraki, Japan
71. H. Berk, Institute for Fusion Studies, University of Texas, Austin, TX 78712
72. I. B. Bernstein, Yale University, 200 Mason Lane, New Haven, CT 06520
73. V. P. Bhatnager, Ecole Royale Militaire, Laboratoire de la Physique des Plasmas, 30 Avenue de la Renaissance, 1040 Brussels, Belgium

74. M. Bornatici, Instituto di Fisica Applicata, Universita di Pavia, Via Bassi 6, 27100 Pavia, Italy
75. R. R. Cano, Service du Confinement des Plasmas, Centre d'Etudes Nucleaires, B.P. 6, 92260 Fontenay-aux-Roses (Seine), France
76. P. Catto, Laboratory for Applied Physics Studies, Science Applications, Inc., P.O. Box 2351, La Jolla, CA 92038
77. V. S. Chan, GA Technologies, Inc., P.O. Box 81608, San Diego, CA 92138
78. P. Colestock, Princeton Plasma Physics Laboratory, P.O. Box 451, Princeton, NJ 08544
79. K. Connor, Electrophysics Division, Rensselaer Polytechnic Institute, Troy, NY 12181
80. CTR Reading Room, c/o A. N. Kaufman, Department of Physics, University of California, Berkeley, CA 94720
81. D. Dobrott, Laboratory for Applied Physics Studies, Science Applications, Inc., P.O. Box 2351, La Jolla, CA 92038
82. Energy Research Center, TRW Defense and Space Systems, 1 Space Park, Redondo Beach, CA 90278
83. I. Fidone, Centre d'Etudes Nucleaires, B.P. 6, 92260 Fontenay-aux-Roses (Seine), France
84. G. E. Guest, Applied Microwave Concepts, Inc., 2210 Encinitas Boulevard, Encinitas, CA 92024
85. J. Y. Hsu, GA Technologies, Inc., P.O. Box 81608, San Diego, CA 92138
86. B. Hui, Naval Research Laboratory, Washington, DC 20375
87. H. Ikegami, Institute of Plasma Physics, Nagoya University, Nagoya 464, Japan
88. C. Karney, Princeton Plasma Physics Laboratory, P.O. Box 451, Princeton, NJ 08544
89. N. A. Krall, Jaycor, P.O. Box 85154, San Diego, CA 92138
90. Library, JET Joint Undertaking, Abingdon, Oxon OX14 3DB, United Kingdom
91. C. Maroli, Association Euratom-CNR, Instituto di Fisica del Plasma, Via Bassini 15, 20133 Milano, Italy
92. G. Morales, Physics Department, University of California, 405 Hilgard Avenue, Los Angeles, CA 90024
93. E. Oktay, Office of Fusion Energy, Office of Energy Research, U.S. Depsrtment of Energy, Mail Station G-238, Washington, DC 20545
94. R. R. Parker, Plasma Fusion Center, 167 Albany Street, Cambridge, MA 02139
95. M. Porkolab, Plasma Fusion Center, 167 Albany Street, Cambridge, MA 02139
96. W. Sadowski, Office of Fusion Energy, Office of Energy Research, U.S. Department of Energy, Mail Station G-238, Washington, DC 20545
97. J. Shearer, Magnetic Fusion Energy, L-382, Lawrence Livermore National Laboratory, P.O. Box 808, Livermore, CA 94550
98. B. Stallard, Magnetic Fusion Energy, L-382, Lawrence Livermore National Laboratory, P.O. Box 808, Livermore, CA 94550
99. S. Tamor, Laboratory for Applied Physics Studies, Science Applications, Inc., P.O. Box 2351, La Jolla, CA 92038

100. T. H. Stix, Princeton Plasma Physics Laboratory, P.O. Box 451, Princeton, NJ 08544
101. J. A. Tataronis, Nuclear Engineering Department, University of Wisconsin, 1500 Johnson Drive, Madison, WI 53706
102. J. Turner, Office of Fusion Energy, Office of Energy Research, U.S. Department of Energy, Mail Station G-238, Washington, DC 20545
103. K. Uo, Plasma Physics Laboratory, Kyoto University, Gokasho-Uji, Kyoto, Japan
104. F. Verdaguer, Division of Fusion, Junta de Energia Nuclear, Madrid 3, Spain
105. M. Wakatani, Plasma Physics Laboratory, Kyoto University, Gokasho-Uji, Kyoto, Japan
106. H. Weitzner, Courant Institute, New York University, 251 Mercer Street, New York, NY 10012
107. M. N. Rosenbluth, University of Texas, Institute for Fusion Studies, RLM 11.218, Austin, TX 78712
108. Theory Department Read File, c/o D. W. Ross, University of Texas, Institute for Fusion Studies, Austin, TX 78712
109. Theory Department Read File, c/o R. C. Davidson, Director, Plasma Fusion Center, NW 16-202, Massachusetts Institute of Technology, Cambridge, MA 02139
110. Theory Department Read File, c/o F. W. Perkins, Princeton Plasma Physics Laboratory, P.O. Box 451, Princeton, NJ 08544
111. Theory Department Read File, c/o L. Kovrizhnykh, Lebedev Institute of Physics, Academy of Sciences, 53 Leninsky Prospect, 117924 Moscow, U.S.S.R.
112. Theory Department Read File, c/o B. B. Kadomtsev, I. V. Kurchatov Institute of Atomic Energy, P.O. Box 3402, 123182 Moscow, U.S.S.R.
113. Theory Department Read File, c/o T. Kamimura, Institute of Plasma Physics, Nagoya University, Nagoya, Japan
114. Theory Department Read File, c/o C. Mercier, Euratom-CEA, Service des Recherches sur la Fusion Controlee, Fontenay-aux-Roses (Seine), France
115. Theory Department Read File, c/o T. E. Stringer, JET Joint Undertaking, Culham Laboratory, Abingdon, Oxon OX14 3DB, England
116. Theory Department Read File, c/o K. Roberts, Culham Laboratory, Abingdon, Oxon OX14 3DB, England
117. Theory Department Read File, c/o D. Biskamp, Max-Planck Institut fur Plasmaphysik, D-8046 Garching bei Munchen, Federal Republic of Germany
118. Theory Department Read File, c/o T. Takeda, Japan Atomic Energy Research Institute, Tokai, Naka, Ibaraki, Japan
119. Theory Department Read File, c/o C. S. Liu, GA Technologies, Inc., P.O. Box 81608, San Diego, CA 92138
120. Theory Department Read File, c/o L. D. Pearlstein, Lawrence Livermore National Laboratory, P.O. Box 808, Livermore, CA 94550
121. Theory Department Read File, c/o R. Gerwin, CTR Division, Los Alamos National Laboratory, P.O. Box 1663, Los Alamos, NM 87545
122-329. Given distribution as shown in TID-4500, Magnetic Fusion Energy (Distribution Category UC-20 f,g: Experimental Plasma Physics and Theoretical Plasma Physics)